Carbohydrates and the oxidative branch of the pentose phosphate pathway modify *Bacteroides thetaiotaomicron* phage resistance by phase variable S-layers.

Jaime J. Fuentes[1], Shaleni Singh[1], Nicholas A. Pudlo[1], Stacey L. Heaver[2], Ruth E. Ley[2], and Eric C. Martens[1]#

[1]Department of Microbiology and Immunology, University of Michigan Medical School

[2]Department of Microbiome Science, Max Planck Institute for Biology, Tuebingen, Germany

Running Head: Carbohydrates modify *B. thetaiotaomicron* phage resistance by S-layer

#Address correspondence to Eric C. Martens, emartens@umich.edu

Abstract

The human gut microbiota consists of hundreds of bacterial species, some of which persist in the presence of lytic phage that infect them. *Bacteroides* employ numerous phase-variable strategies to survive in the presence of phage, including capsular polysaccharides (CPS) and S-layer lipoproteins. We previously reported that a *Bacteroides thetaiotaomicron* strain lacking CPS exhibits almost complete resistance to multiple phages when forced to express the S-layer protein BT1927. However, this strain was only resistant after certain growth conditions, suggesting nutritional variables alter infection and resistance. We grew this strain on various simple sugars and polysaccharides finding that some substrates (fructose, glucose) promote strong resistance to a single phage (ARB25) while others like *N*-acetylgalactosamine (GalNAC) and mucin *O*-glycans increase susceptibility. Mixing fructose and GalNAc indicates the effects of GalNAc are dominant. Despite increasing ARB25 susceptibility, GalNAc did not reduce *BT1927* transcript or protein levels. Instead, GalNAc reduced the amount of BT1927 displayed on the cell surface and increased outer membrane vesiculation. Mutants in any of the 3 steps of the oxidative branch of the pentose phosphate pathway—grown in fructose—behaved similarly to wild-type cells grown in GalNAc, illuminating this pathway in regulation of sugar-mediated phage-resistance. Despite promoting strong resistance, cells grown in glucose/fructose sometimes displayed sub-populations that appeared to completely lack surface BT1927, suggesting another checkpoint exists to control whether this phage defense is deployed. Finally, we show the mucin sugar GalNAc increases susceptibility to several other phage, which has implications for *B. thetaiotaiomicron* persistence in niches like the mucus layer.

42 **Importance**

43 The persistence of viruses that infect bacteria (bacteriophages or phages) in the
44 human gut microbiome and their effects on bacterial physiology and host health are
45 active areas of investigation. Our study investigates how various sugars and
46 polysaccharides alter phage susceptibility and resistance in the model gut symbiont
47 *Bacteroides thetaiotaomicron* to lytic phages that are capable of infecting it. Our finding
48 that the mucin sugar, *N*-acetylgalactosamine, and mucin *O*-glycans that contain this
49 sugar reduce *B. thetaiotaomicron* resistance to multiple phages has implications for
50 how this symbiont persists in different gut microhabitats, such as the mucus layer, and
51 which defense mechanisms it can deploy to survive in these niches.
52

53 **Introduction**

54 The human gut is home to a community of symbiotic microbes (microbiome) that
55 impart beneficial functions to their host, including digestion and metabolism of nutrients
56 like complex carbohydrates (1, 2), immune stimulation (3–5), and protection against
57 pathogens (6, 7). Individual bacterial species that compose the microbiome often
58 encounter perturbations, including changing diet, severe osmotic stress, immune
59 responses, antibiotics and exposure to bacteriophages (herein, phages) (8–13), all of
60 which could limit the ability of individual bacteria to persist in the community. Phages are
61 the most abundant biological entities in the human gut (14) and target specific species.
62 The presence of phage could have consequences for microbiome composition, as well
63 as the host, if they were able to eradicate their target bacterial species and eliminate its
64 beneficial functions. Further, phage could disrupt community stability by eliminating their
65 target species and indirectly reducing beneficial functions provided by bacteria that rely
66 on the phage-targeted species (15, 16). Despite the potential for phage to cause such
67 disruptions, longitudinal human studies indicate that most bacterial strains are stable for
68 long periods (9, 17, 18). A notable experiment in which phage were administered to
69 gnotobiotic mice colonized with a community of human bacteria demonstrated that
70 although specific bacterial species experienced transient reductions in abundance, their
71 abundance later recovered, and their target phage were eliminated or reduced below
72 detection limits (19). Notably, both bacterial species that survived this phage challenge
73 were members of the genus *Bacteroides*, which is particularly prominent in the
74 microbiomes of people from industrialized countries. This study reveals that at least

75 some gut bacteria have mechanisms to persist in the gut ecosystem despite the
76 presence of phage that prey on them.

77 Indeed, mechanisms through which gut bacteria resist phage infection and their
78 effect on microbiome stability are emerging. Metagenomic and functional studies have
79 detected a number of known or previously unknown phage resistance mechanisms in
80 gut microbiome species such as: clustered regularly interspaced palindromic repeat
81 (CRISPR) arrays (20–22), cyclic oligonucleotide-based antiphage signaling systems
82 (CBASS) (22–24), restriction-modification systems (22, 25), and variation of cell surface
83 structures like capsular polysaccharides (CPS) and surface layer lipoproteins (S-layers)
84 (22, 26, 27). While mechanistic characterization of these systems is ongoing (20), few
85 have been examined through the lens of regulation in response to the bacterial cell's
86 nutritional status.

87 Phase-variation is a reversible phenomenon that often involves DNA inversion of
88 the promoter that directs transcription of a specific gene or operon, such that some cells
89 in a population express the gene and others do not. We previously reported that the
90 model human gut symbiont, *Bacteroides thetaiotaomicron*, is able to resist phage
91 infection through phase-variable expression of CPS biosynthetic loci, candidate S-layer
92 proteins, restriction-modification, and lipoprotein systems (27). Some of these systems
93 have since been reported to be important for phage resistance in other *Bacteroides*
94 species (28, 29). The presence of these phase-variable systems enables *B.*
95 *thetaiotaomicron* to "pre-adapt" some members of its population to survive phage
96 infection because resistant cells, which already exist in a population (*i.e.*, they have
97 turned on one of the mechanisms noted above), survive and become dominant when

98 phages are present. Interestingly, the reversibility of these systems continuously
99 generates susceptible cells that may be killed by phage and potentially sustain the viral
100 population (27), a phenomenon observed decades ago in some *Bacteroides* species
101 and referred to as a “carrier culture” state or pseudolysogeny, although the latter term
102 has been used to refer to different phenomena more recently (30, 31). The presence of
103 reversible phage resistance mechanisms is likely a result of constant coevolutionary
104 adaptation by bacterial species and could result in long-term persistence of phage
105 populations within the gut along with their host bacteria. Consistent with this, phage
106 populations in some human studies have been observed to be stable for at least 1 year
107 (32, 33).
108 S-layer lipoproteins are ubiquitous among both Gram-positive and Gram-
109 negative bacteria and are characterized by a proteinaceous crystalline-like surface
110 structure (34, 35). Previous work characterized a functional role for one phase-variable
111 *B. thetaiotaomicron* S-layer protein (encoded by the *BT1927* gene), which was
112 visualized as a crystalline-like surface structure by electron microscopy when the
113 *BT1927* gene was expressed (35, 36). *BT1927* transcription is mediated by a phase-
114 variable promoter flanked by invertible repeats that mediate recombination and
115 inversion of the promoter since mutation of one of the two inverted repeats can “lock”
116 the promoter in the ON or OFF position. Antibody staining demonstrated that the
117 BT1927 S-layer gene is expressed in about 1 in 1,000 wild-type cells grown *in vitro* in
118 rich medium (*i.e.*, in the absence of phage), while human metagenomic analysis
119 indicated that the promoter-on frequency is higher *in vivo*. While this first study of
120 BT1927 did not test for a role in phage resistance, it reported that BT1927 promotes

121 resistance to complement-mediated killing (36). In our previous study of *B.*
122 *thetaiotaomicron* phage resistance, increased transcription of *BT1927* in response to
123 phage challenge was a prominent response in the absence of CPS, suggesting it
124 promotes phage resistance. Consistent with this, a strain in which BT1927 was locked
125 on demonstrated nearly complete resistance to at least four phages (27). However, this
126 resistance was only observed when colonies were “aged” for three or more days on
127 solid medium with glucose as the primary carbon source prior to culture in liquid
128 medium. This age-variable resistance occurred even though transcription of the BT1927
129 gene was locked on, suggesting that growth conditions related to colony aging could
130 either modify the transcriptional output of the *BT1927* promoter or act post-
131 transcriptionally to modify BT1927 effects.

132 *B. thetaiotaomicron* is adept at harvesting carbohydrates from a variety of diet
133 and host polysaccharides, which are a significant nutrient source for this species
134 compared to protein (37–41). In this study, we measured how the different
135 carbohydrates utilized by *B. thetaiotaomicron* impact the ability of the BT1927 S-layer to
136 promote phage resistance when the *BT1927* gene is constitutively expressed. We found
137 that *B. thetaiotaomicron* exhibits variable resistance to a single lytic phage, when
138 cultured in liquid medium containing one of 27 different individual carbohydrates (simple
139 sugars and polysaccharides). We also discovered that steps in the oxidative branch of
140 the pentose phosphate pathway are important for full phage resistance via BT1927
141 expression. The carbohydrates that reduced BT1927-mediated resistance most were
142 the sugar *N*-acetylgalactosamine (GalNAc) and mucin *O*-glycans that contain this sugar.
143 Interestingly, decreased phage resistance did not correlate with reduced BT1927

144 transcription or protein abundance in the cell, but was associated with less BT1927
145 protein on the cell surface and increased production of outer membrane vesicles
146 (OMVs) that may disrupt the integrity of this protective S-layer. Because the
147 carbohydrate-based nutrients available to gut bacteria frequently change with variations
148 in host diet, thereby influencing their cellular responses, our findings have important
149 implications for understanding how the stability and co-existence of bacteria and phage
150 populations in the human gut may be influenced by diet or bacterial occupation of
151 niches like the colonic mucus layer.
152
153

Results

Carbohydrates influence BT1927 S-layer mediated phage resistance

The nutritional environment experienced by a bacterial cell, such as the presence of specific nutrients or nutrient deprivation, has potential consequences for interactions with phage. Two classic examples of bacterial nutrient exposure that modify phage susceptibility in *E. coli* are the presence of maltose or iron-deficient conditions, each of which induces expression of a cognate phage receptor (LamB or FhuA, respectively) (42, 43). Given the previously determined requirement for “aging” BT1927-expressing cells for three days to elicit strong protection against ARB25 phage, we hypothesized that an unknown nutrient signal(s) alters the ability of BT1927 to protect against phage. Consistent with our previous observations (27), when a strain with the phase-variable *BT1927* promoter genetically locked-on (herein, BT1927:ON) was aged for 3 days and infected with ARB25, it exhibited similar growth as a heat-killed phage control when infections were performed in media containing glucose (**Figure 1A**). This protection against ARB25 was dependent on both locked expression of BT1927 and colony aging, since both a BT1927 locked-off strain (BT1927:OFF) and the BT1927:ON strain grown without aging achieved significantly lower growth ($P<0.0001$) at 24 hours and generally failed to maintain the same high density as the BT1927:ON aged strain in the first ~40 hours of infection (**Figure 1A, B**, compare red and blue curves to green). Growth eventually increases later after infection with many strains or conditions, likely driven by the emergence of cells expressing other phase-variable resistance proteins, of which there are 7 known to exist in the engineered strain used here.

176 Consistent with previous work (36), scanning electron microscopy (SEM) imaging
177 of the BT1927:OFF strain did not reveal a lattice structure on the outside of the cell
178 (**Figure 2A**). However, individual BT1927:ON cells did display a surface lattice that is
179 similar to what has been previously observed (**Figure 2B).** Interestingly, images of a
180 phage-free culture of the BT1927:ON strain grown in medium with glucose as the main
181 carbohydrate source contained a population of ~60% of cells that appeared to display
182 the lattice structure on the majority of the cell surface while the remaining individual
183 cells appeared mostly devoid of this structure, suggesting that there may be variation in
184 the expression of the BT1927 S-layer at the single cell level (**Figure 2C, Figure S1A**).
185 To explore how the aged colony, high ARB25-resistance phenotype persists over
186 time with repeated liquid culture, aged colonies were grown in liquid BPRM glucose,
187 allowed to grow for 24 hours, and sub-cultured 1:100 each day for 5 days. Each day, a
188 portion of the culture grown in BPRM glucose for the previous 24 hours was also sub-
189 cultured and subjected to ARB25 infection (MOI 0.5). Interestingly, we found that
190 passaging of cultures for two days or longer in liquid BPRM-glucose medium was
191 sufficient to promote strong resistance even when starting with cultures of BT1927:ON
192 that had not been grown on solid medium (**Figure 3A, Figure S1B, C**). This observation
193 suggests that multiple generations of growth in glucose—and not necessarily aging on
194 plates—is sufficient to increase the effect of BT1927 to protect against ARB25. Given
195 that glucose is used as the sole carbohydrate source in the media that promoted this
196 phenotype, we aimed to determine how other dietary carbohydrates might alter BT1927-
197 mediated resistance as carbohydrates are the major group of nutrients used by *B.*
198 *thetaiotaomicron*. We leveraged a panel of 14 monosaccharides and 13

199 polysaccharides that support the growth of *B. thetaiotaomicron* when present as sole
200 carbon sources and measured growth dynamics of the BT1927:ON strain during
201 infection with ARB25 phage. Briefly, the BT1927:ON strain was grown on BPRM solid
202 agar medium containing glucose for three days, colonies were cultured in liquid BPRM
203 glucose, allowed to grow for ~20 hours, and sub-cultured into BPRM containing each
204 carbohydrate followed by phage challenge (**Figure S1D**).

205 Several of the carbohydrates in our panel resulted in growth in the presence of
206 ARB25 that was similar to glucose. For example, fructose also promoted a strong and
207 uninterrupted early growth increase in the presence of ARB25 (**Figure 3B, Figure S2A**).
208 In contrast, other carbohydrates elicited growth in the presence of ARB25, that was
209 more similar to the unaged or BT1927:OFF strain grown in glucose (**Figure 1A**). For
210 example, growth in medium containing *N*-acetylgalactosamine (GalNAc) led to an initial
211 growth increase after ARB25 exposure that was blunted and remained low for the first
212 ~40 hours after initial infection (**Figure 3C**). This low early growth on GalNAc suggests
213 that, in contrast to glucose and fructose, GalNAc fails to promote and perhaps even
214 suppresses BT1927-mediated resistance. As observed with unaged or unpassaged
215 colonies, cultures in GalNAc eventually gained in absorbance (**Figure 3C**), likely due to
216 the emergence of cells that express other resistance mechanisms. Our previous study
217 demonstrated that up to 10 different phase-variable systems (excluding polysaccharide
218 capsules) could be expressed *in vitro* in the presence of ARB25 challenge (27): 8
219 putative S-layers (including BT1927), a restriction-modification system and a single
220 locus encoding 3 lipoproteins different from the S-layers. Therefore, we probed
221 transcription of these nine other phase-variable systems, plus locked on *BT1927*, during

222 growth in GalNAc and fructose and in the presence of ARB25. This experiment revealed
223 that fructose promoted the emergence of cells with increased transcription of the genes
224 encoding the seven other S-layers, the restriction-modification system (*BT4013-15*) and
225 the additional lipoprotein locus (*BT0291-94*). This suggests that these different systems
226 may confer additional or better protection beyond BT1927 and are therefore selected
227 later in culture in the presence of ARB25. Interestingly, five of the nine systems
228 expressed in fructose had significantly lower expression in GalNAc, and one gene
229 encoding a candidate S-layer (BT1507) was expressed at significantly higher levels in
230 GalNAc (**Figure S2B, C**). These results support the conclusion that different sugars
231 modify the range of phage resistance responses that emerge in a population, possibly
232 by modifying the effectiveness of each specific mechanism during growth in a given
233 sugar.

234 Since we observed a range of responses to ARB25 during early infection on
235 different carbohydrates, we quantified the difference between heat-killed and ARB25
236 infected cultures using 24-hours as a common "early" time point (delta symbols in
237 **Figures 3B, C** indicate examples of the growth difference measured for each
238 carbohydrate). Ranking the effects of individual carbohydrates revealed a continuum of
239 effects on BT1927-mediated resistance, with the previously mentioned fructose and
240 GalNAc exhibiting the highest and lowest resistance, respectively (**Figure 3D**). The
241 effects of monosaccharides tended to be stronger than polysaccharides at reducing
242 BT1927-mediated resistance, although both groups showed a broad range of
243 responses. The polysaccharide that resulted in the most reduced resistance to ARB25
244 was mucin *O*-glycans (MOG), a mixture of oligosaccharides that interestingly contains

245 the monosaccharide GalNAc (**Figure 3E**). Other monosaccharides present in MOG
246 (galactose, fucose, and *N*-acetylglucosamine) did not increase susceptibility to ARB25
247 to the same level as GalNAc, although the latter two sugars elicited strong susceptibility
248 in some experiments (**Figure S1D**). There was also discordance between the effects of
249 glucose and the four polymers that contain glucose (dextran, pullulan, glycogen, and
250 amylopectin). Thus, we cannot conclude that polysaccharides universally exert the
251 same effect as the monosaccharides they contain. Since we determined that MOG and
252 GalNAc reduce resistance to ARB25, we tested 5 other phages, finding that growth in
253 these two carbohydrates also reduced resistance to 4 of the phages tested when
254 cultured similarly to the experiments described above with ARB25 (**Figure S2D**).
255 Given the disparate effects of fructose and GalNAc on resistance to ARB25, we
256 aimed to determine if the strong resistance developed after passage in a medium
257 containing glucose could be reversed by the addition of carbohydrates like GalNAc and
258 if one sugar-associated phenotype is dominant over the other. Passage of cultures in
259 glucose for five days, which promoted strong ARB25 resistance, followed by a shift to
260 GalNAc, decreased growth in the presence of ARB25 (**Figure S3A**), demonstrating that
261 GalNAc can induce increased ARB25 susceptibility in cultures that previously exhibited
262 resistance and consequently suggesting that the resistance is not permanent as would
263 be expected for genetic mutation in the ARB25 receptor or other function required for
264 infection. Continuous passage in GalNAc for 5 days resulted in slightly more blunted
265 growth, suggesting a potential compounding effect. In contrast, passage in fructose
266 resulted in continued strong resistance as indicated by lower difference in maximum
267 absorbance between infected and uninfected bacteria (**Figures 4A, S3A,** note that the

268 resistance at 24h for fructose in this experiment may be underrepresented at some days
269 due to some of the uninfected conditions increasing absorbance on this sugar after the
270 initial entry into stationary phase).

271 To address whether fructose or GalNAc are dominant, we passaged cultures in
272 medium containing equal amounts of fructose and GalNAc (5mg/ml each). This resulted
273 in growth that was very similar to GalNAc grown cultures, suggesting that the effect of
274 GalNAc is dominant over that of fructose (**Figure 4A, Figure S3A**). We next determined
275 whether growth on solid medium with GalNAc for 3 days resulted in increased ARB25
276 susceptibility after cells were grown in liquid medium and exposed to phage. Consistent
277 with our results in liquid medium, cultures from colonies picked from agar containing
278 glucose, first cultured in BPRM glucose, and then infected in BPRM GalNAc showed
279 lower resistance at 24h but later increased growth (**Figure S3B**). In contrast, growing
280 BT1927:ON strain on GalNAc agar plates and subsequently in liquid BPRM GalNAc for
281 growth and infection resulted in cultures that were more susceptible at 24h and failed to
282 increase growth as much as glucose grown cells at later times (**Figure S3C**). This latter
283 result supports our conclusions from repeated culture in liquid medium that previous
284 exposure to glucose exerts an effect that persists for some amount of time after first
285 exposure to GalNAc and this influences how the cells resist ARB25 infection.

286 We next measured if growth in medium containing fructose or GalNAc alters the
287 plaquing efficiency of ARB25 on the BT1927:ON strain, which could explain the
288 apparently high and low ARB25 resistance trends we observed in liquid cultures.
289 Consistent with our results in liquid media, plaquing efficiency was significantly higher in
290 GalNAc-containing plates compared to those containing fructose and the GalNAc

291 medium promoted a similar number of plaques on the BT1927:ON strain as the parent
292 acapsular strain—which does not have BT1927 locked on—grown on fructose (**Figure**
293 **4B**). Moreover, plaques appeared less turbid in the GalNAc medium compared to
294 glucose, potentially indicating that this sugar increases the efficiency of ARB25 infection
295 of individual cells as waves of post-infection phage bursts encounter new prey in their
296 surroundings (**Figure 4C**). Similar to earlier studies showing that the BT1927 locked-on
297 strain is protected against complement killing compared to the locked-off strain in
298 medium containing glucose (36), cultures grown in GalNAc exhibited significantly
299 reduced survival compared to fructose grown cells when exposed to complement
300 (**Figure S3D**). These data further suggests that the protective nature of the BT1927 S-
301 layer is influenced by the specific carbohydrates encountered by the cell.
302
303 **N-acetylgalactosamine reduces BT1927 expression on the bacterial surface**
304 We next determined if cultures of BT1927:ON grown in fructose or GalNAc
305 exhibit variations in surface exposed BT1927. We used flow cytometry to measure
306 surface expression of a previously published BT1927 variant with a FLAG epitope
307 appended to the C-terminus (36) (BT1927:ON^{F}). To first determine if the presence of the
308 FLAG epitope disrupts BT1927 function with respect to surviving phage, we challenged
309 cultures of the BT1927:ON^{F} strain with ARB25 and determined that it maintains
310 resistance when cultured in fructose (**Figure S3E)**. We then performed flow cytometry
311 using the BT1927:ON^{F} strain grown in fructose or GalNAc to mid-log phase. Using an
312 antibody against the FLAG epitope, the BT1927:ON^{F} strain grown in fructose could be
313 clearly distinguished from the BT1927:OFF strain grown in the same medium by flow

314 cytometry (**Figure 5A**). The BT1927:ON^F strain grown in GalNAc was clearly different
315 from fructose-grown cultures and had less intense staining overall with an average
316 geometric mean fluorescence intensity of 200$\pm$62 (GalNAc) versus 578$\pm$64 (fructose; P
317 = 0.0017, one tailed t-test), although it was also clearly increased relative to the
318 BT1927:OFF control (**Figure 5A)**. This result suggests that GalNAc-grown cells express
319 less BT1927 on the cell surface.
320 An interesting observation in several repetitions of this experiment, was the
321 presence of a distinct population of BT1927:ON^F cells that stained similarly to the
322 BT1927:OFF control population after cultivation in fructose (**Figure 5B** small
323 histograms**, Figure S4A**). In the first experiment in which this occurred (**Figure S4A**), all
324 three biological replicates were similar to each other while in our first experiment all
325 three replicates lacked this population (**Figure 5A**). We interpret this observation to
326 indicate that in some cases, a population of cells can be present that expresses very
327 little cell-surface associated BT1927 despite the fact that expression is locked on and
328 the growth sugar (fructose) promotes overall strong ARB25 resistance in the population.
329 We do not suspect that this is a technical artifact (*e.g.*, poor antibody labeling in the
330 experiment with a prominent BT1927 low population) because the BT1927 high
331 populations displayed similarly high staining intensity. Instead, this bimodal population
332 of BT1927-expressing cells could reflect the two populations of cells that we initially
333 observed by SEM imaging of cells grown in glucose (**Figure 2C**). If true, these two
334 observations would support the conclusion that *B. thetaiotaomicron* possesses a switch
335 or decision-making mechanism that governs the fate of individual cells to express
336 BT1927 (and perhaps other proteins) on the cell surface. To further investigate variation

337 in BT1927 expression between experiments with growth in fructose, we grew the
338 BT1927:ON^{F} strain in several different anaerobic chambers with each replicate
339 cultivated from a different starting colony. Among the four experiments, one exhibited a
340 low staining population of BT1927:ON (**Figure S4B**), supporting the conclusion that this
341 is a repeatable phenomenon that could be driven by an unknown environmental
342 stimulus or stochastic variation in *B. thetaiotaomicron* cell populations. Since our
343 previous data indicated that GalNAc was dominant in decreasing the resistance of the
344 BT1927:ON strain to ARB25 when fructose was also present, we grew the BT1927:ON^{F}
345 strain in media containing both fructose and GalNAc to measure BT1927 expression
346 levels. Strikingly, the BT1927:ON^{F} strain grown in a mixture of fructose and GalNAc was
347 clearly distinct from fructose-grown cultures, had less intense staining overall and was
348 very similar to cells grown only in GalNAc (**Figure 5B**). This observation suggests that
349 the effect of GalNAc is dominant over fructose and may not allow maximum expression,
350 asembly or retention of BT1927 on the cell surface.
351 Since GalNAc reduces the amount of surface associated BT1927 protein, we
352 next sought to determine at which point in expression this effect is exerted. Since the
353 *BT1927* promoter is already locked in the phase-variable “on” position, we measured if
354 transcription of the *BT1927* S-layer is downregulated upon exposure to GalNAc.
355 Comparison of the BT1927:ON strain in GalNAc or fructose (in the absence of phage)
356 revealed that *BT1927* transcript was not diminished by GalNAc (**Figure 5C**). Similarly,
357 high *BT1927* transcription was observed during growth on another carbohydrate,
358 glucosamine, that increases ARB25 susceptibility (**Figure S4C**) Next, we performed a
359 western blot on the BT1927:ON^{F} strain grown in media containing either fructose or

360 GalNAc to assess BT1927 protein levels in whole cells. BT1927 protein did not appear
361 to be different between fructose and GalNAc grown cultures (**Figure S4D**), although the
362 western blot was not performed quantitatively and is unlikely to discriminate between
363 small changes in protein expression that might explain the partial reduction in surface
364 staining observed by flow cytometry. To more quantitatively determine if these two
365 sugars alter BT1927 protein abundance, we performed proteomics using LC-MS/MS to
366 measure the relative normalized protein abundance of BT1927 in the BT1927:ON strain
367 grown in either fructose or GalNAc. The abundance of BT1927 was not significantly
368 decreased by growth in GalNac compared to fructose (**Figure 5D)**. As a control for
369 expected sugar-specific responses, growth in fructose led to a 1.6-5.0-fold increase in
370 five of the eight individual proteins encoded in a previously identified polysaccharide
371 utilization locus (PUL) for the fiber levan that is upregulated in response to fructose (44)
372 (**Figure S4E**). Taken together, although GalNAc increases ARB25 susceptibility and
373 decreases its abundance on the cell surface, we do not have any evidence that GalNAc
374 reduces transcription or translation of the BT1927 lipoprotein, which therefore
375 necessitates that lack of surface expression must either occur at the level of BT1927
376 secretion or trafficking to the outer leaflet of the membrane, its folding to form an
377 effective S-layer or its retention on the cell surface. Interestingly, when we performed
378 additional SEM to attempt to visualize the BT1927 lattice on the *B. thetaiotaomicron*
379 surface (which proved difficult to resolve using the instruments available at the
380 University of Michigan), we noticed a substantial increase in what appeared to be outer
381 membrane vesicles in the supernatant surrounding the *B. thetaiotaomicron* cells (**Figure**
382 **5E, F).** *B. thetaiotaomicron* and other *Bacteroides* have been actively investigated in

383 recent years because of their prolific ability to not only produce OMVs but also regulate
384 this process either positively or negatively (45, 46). Quantification of OMVs by a
385 previously published method (47) using the images of fixed and whole-mounted
386 bacterial cultures (with medium supernatant) revealed that growth in GalNAc increases
387 the number of extracellular OMVs ~25-fold (**Figure 5E, S4F, G**). Thus, while we were
388 unable to visualize the BT1927 lattice with sufficient resolution after growth in fructose
389 and GalNAc, our data suggest that GalNAc induces increased vesiculation by this
390 species which could interfere with the ability of BT1927 to block phage infection.

391 **The oxidative branch of the pentose phosphate pathway regulates susceptibility**
392 **to phage**

393 Carbohydrate utilization by *B. thetaiotaomicron* and other *Bacteroides* is a highly
394 regulated process involving multiple layers of regulation. Polysaccharide utilization
395 occurs via expression of substrate-specific PULs and these gene clusters typically
396 exhibit large increases in transcription (50 to >1,000-fold) in response to their target
397 polysaccharide (48). PUL regulation is most commonly mediated by locally acting,
398 positive-acting transcription factors (1). However, global regulatory phenomena—which
399 are still incompletely understood—also exist to control both polysaccharide and
400 monosaccharide utilization in *B. thetaiotaomicron* and at least polysaccharide utilization
401 is subjected to catabolite repression-like effects (*i.e.*, some polysaccharides are given
402 high priority while utilization of others is repressed until favored substrates are depleted)
403 (49). Several features involved in global regulation have emerged in recent years, one
404 being a homolog of the *E. coli* catabolite repression protein (CRP) currently referred to
405 as carbohydrate utilization regulator (Cur, previously MalR, *BT4338*). Cur is a global

406 regulator that is required for the normal utilization of multiple poly- and
407 monosaccharides and is thought to work independently of cAMP, which has not been
408 observed in *Bacteroides* (50). Mutants in the oxidative branch of the pentose phosphate
409 pathway (PPP), including 6-phosphogluconate dehydrogenase (BT1222), have been
410 discovered in multiple studies to play a role in polysaccharide or glucosinolate
411 utilization, because these mutants fail to properly express the corresponding PULs or
412 their regulators (50–52). One study found that mutants lacking either functional Cur or
413 the oxidative PPP both fail to fully express a hybrid two component system regulator
414 (Roc) involved in mucin *O*-glycan utilization, implying that these two features may
415 overlap at least partially (50). Interestingly, Roc expression, which is Cur-dependent, is
416 suppressed by glucose and fructose, the two sugars that promote the highest resistance
417 to ARB25.

418 To determine whether mutants in the PPP or Cur influence ARB25 resistance, we
419 measured growth of four previously identified transposon mutants with disrupted genes
420 in the oxidative branch of the PPP (in the same strain background lacking all 8 capsular
421 polysaccharides used for other experiments in this study). These mutants, which do not
422 have the *BT1927* promoter locked on, exhibited impaired growth relative to the
423 untreated acapsular *B. thetaiotaomicron* strain when infected with ARB25, suggesting a
424 deficiency in deployment of the multiple phase-variable mechanisms that it still retains,
425 including BT1927 (**Figure 6A, Figures S5A-E**). In light of these findings, we evaluated
426 the effects of deleting the *BT1222* gene, encoding the terminal step in the oxidative
427 branch of the PPP, in the BT1927:ON strain. Deletion of *BT1222* resulted in diminished
428 resistance to ARB25 compared to the uninfected control when grown in fructose (**Figure**

429 **6B**). Consistent with its apparent increased susceptibility in liquid medium containing
430 fructose, the Δ*BT1222* BT1927:ON strain displayed an increased number of plaques
431 compared to the BT1927:ON parent, albeit less than the parent acapsular strain when
432 both were grown in medium with fructose (**Figure S5F**). Given the increased
433 susceptibility associated with deletion of *BT1222*, we measured *BT1927* transcript
434 levels and confirmed that expression remained unaltered in the Δ*BT1222* mutant
435 (**Figure 6C**). Similar to GalNAC grown cells that showed increased ARB25
436 susceptibility, we also did not see an appreciable decrease in BT1927 protein by
437 western blot (**Figure S5G**). Finally, using flow cytometry, we observed a decrease in
438 BT1927 surface staining when the Δ*BT1222* BT1927:ON^{F} strain was grown in fructose
439 (**Figure 6D**).
440 We next examined the role of the global regulator Cur, which appears to share
441 some regulation in common with the enzymes in the oxidative branch of the PPP (50).
442 Mutants in which the gene encoding Cur (*BT4338*) was deleted in the Dcps or
443 BT1927:ON backgrounds did not increase susceptibility during growth in fructose as
444 substantially as the PPP mutants, although some increased ARB25 susceptibility was
445 observed (**Figure S5H, I).** Consistent with this, flow cytometry of the epitope-tagged
446 BT1927:ON^{F} strain lacking Cur also displayed similarly intense staining as the parent
447 strain grown in fructose (**Figure S3J**) with an average geometric mean fluorescence
448 intensity of 293$\underline{+}$60 (BT1927:ON^{F}) and 209$\underline{+}$44 (Δ*BT4338* BT1927:ON^{F}, P value = 0.32).
449 Taken together, we conclude that the presence of an intact oxidative branch of the PPP
450 is required for fructose- and BT1927-mediated phage resistance, but Cur appears to
451 play a less substantial contribution.

452 **Discussion**

453 Phages are the most numerous biological entities in many microbial
454 environments, including the human gut (53). The presence of at least some individual
455 phage is stable over time (54), raising the question of how phage can remain present
456 without eradicating their host bacteria or being lost when their host gains resistance.
457 While several mechanisms like lysogeny and pseudolysogeny factor into these
458 relationships, multiple *Bacteroides* species have been shown over the last several
459 decades, using both *in vitro* and *in vivo* experiments, to co-exist with lytic phage in a
460 state where neither completely wins or loses (27, 30). This phenomenon is driven by the
461 existence of phase-variable resistance mechanisms that presumably are selected for in
462 their "on" state when phage are present but revert to the "off" state at a sufficient
463 frequency to continuously generate susceptible prey bacteria to be infected and
464 replenish phage populations. Indeed, in our previous work we showed that ARB25
465 phage could persist in the colons of *B. thetaiotaomicron* monoassociated mice for over
466 two months, suggesting that reversion of resistant bacteria back to a susceptible state
467 could be sufficient to promote stability of phage populations over longer periods (27). In
468 this study, we bypassed the contributions of phase-variation by locking BT1927
469 expression in the on state and observed additional, sugar-mediated contributions to *B.*
470 *thetaiotaomicron* survival, revealing another layer of regulation that influences phage
471 resistance.

472 The carbohydrate landscape in the mammalian gut is complex and dynamic and
473 also directly influences the metabolism of the bacteria that compose the gut microbiota.
474 Diet is a major external force that shapes the microbiota because dietary fiber—which

475 mostly encompasses plant-derived polysaccharides other than soluble starch—is the
476 major fraction of human foods that reach the colon unabsorbed or undigested by human
477 enzymes (1, 40). *B. thetaiotaomicron* is a nutritional generalist that can utilize a variety
478 of dietary fibers but also has the ability to consume the diverse *O*-glycans attached to
479 secreted gastric and colonic mucin (39, 55). We have previously shown that most
480 dietary fiber polysaccharides that are accessible by *B. thetaiotaomicron* repress
481 expression of this organism's PULs involved in mucin *O*-glycan degradation through a
482 phenomenon resembling carbon catabolite repression (49). When dietary fiber is
483 withheld from *B. thetaiotaomicron* colonized gnotobiotic mice, there is increased
484 expression of PULs involved in *O*-glycan utilization (41, 56) and measurably increased
485 mucus consumption that manifests as thinner colonic mucus (57). Combined with the
486 results presented here, these observations raise the idea that low dietary fiber could
487 force *B. thetaiotaomicron* into conditions that make it more susceptible to phage
488 predation, such as utilization of *O*-glycans and GalNAc, which both increase its
489 susceptibility to phage like ARB25 (**Figure 3D, E**). This increased susceptibility occurs
490 even though *B. thetaiotaomicron* possesses alternative, mainly phase-variable
491 strategies to resist phage (capsular polysaccharides, putative S-layers, plus others).
492 Indeed, we demonstrate with a broader set of phages that infect *B. thetaiotaomicron,*
493 that GalNAc induces an apparent state of increased susceptibility as judged by reduced
494 growth over time in the presence of several phages (**Figure S2D**), a phenomenon that
495 could be mediated by the increased vesiculation that we note during growth in GalNAc
496 (**Figure 5E, F**). Moreover, we show that increased or decreased susceptibility is
497 entrained by prolonged exposure to different sugars like fructose or GalNAc, revealing

498 that the recent “nutritional history” experienced by *B. thetaiotaomicron* may also play a
499 role. The mechanism(s) through which this nutritional memory occurs remains unknown,
500 although some candidates are noted below, but will be important to investigate and may
501 influence other aspects of *B. thetaiotaomicron* physiology.

502 Perhaps one of the most unexpected observations in this study, is the detection
503 of what appear to be cell fate decisions in *B. thetaiotaomicron* that are manifest at the
504 single cell level. Evidence to support this comes first from SEM imaging of BT1927:ON
505 and BT1927:OFF strains and the observation that as many as ~40% of BT1927:ON
506 cells lack the lattice-like surface structure that was previously associated with BT1927
507 expression and instead resemble the BT1927:OFF strain. Additional evidence to
508 support this idea comes from the observation that some cultures of the BT1927:ON^{F}
509 strain grown in fructose harbor a significant population of cells that resemble the
510 BT1927:OFF by flow cytometry. It has been widely reported that *Bacteroides* species
511 encode a variety of mechanisms to generate phenotypic diversity in the population (27,
512 58–60). This diversity pre-adapts sub-populations to survive challenges like host innate
513 and adaptive immune responses and phage. In addition to the phase-variable CPS, S-
514 layer, and other functions noted above, which directly impact resistance to phage and
515 immune components, additional phase-variable events include the existence of phase-
516 variable DNA methylation systems (58) that alter a variety of cell features on a global
517 scale, including CPS expression. While these systems have only been investigated in *B.*
518 *fragilis*, *B. thetaiotaomicron* has two copies of the locus encoding this system (*BT4516-*
519 *4523* and *BT4535-BT4543*) and likely exhibits similar epigenetic regulation via
520 methylation. In addition, phase-variable gene shufflons that diversify the particular

521 nutrient receptors that are expressed via a single transcription factor exist in *B.*
522 *thetaiotaomicron* (58). Indeed, we previously observed a pronounced shift in one of
523 these nutrient receptor shufflons *in vitro* after *B. thetaiotaomicron* was exposed to
524 ARB25 and a resistant cell population was allowed to emerge. Such events that directly
525 alter the identities of nutrient receptors on the cell surface could impact phage infection
526 by modifying receptors and co-receptors that mediate adsorption. Although, it is
527 important to note that a test of this hypothesis for ARB25 and the nutrient receptors that
528 we observed to shift upon infection (by deleting the genes involved) did not support a
529 direct role as the ARB25 receptor. Finally, a recent study demonstrated the presence of
530 much more prevalent DNA inversions (372 different "inverton" events) within the *B.*
531 *thetaiotaomicron* genome and these often occur within coding sequences and are not
532 associated with known recombinases that mediate the inversion (61). While it remains
533 to be investigated, this large amount of genomic variation holds the potential to record
534 aspects of the nutritional memory that we report here, for example, by shifting the
535 genome organization into a different methylation or recombination state that then takes
536 time to shift back when cells encounter another substrate.
537 It is further surprising that the presence of BT1927 on the cell surface is not
538 regulated at the transcriptional or translational levels, which are more traditional control
539 points to conserve energy. Because cellular levels of BT1927 are very similar during
540 growth in fructose and GalNAc, and only fructose-grown cells are capable of displaying
541 the highest amounts of surface BT1927 staining, this necessitates that GalNAc either
542 reduces the efficiency of BT1927 trafficking to the cell surface or causes it to be
543 released from the surface once it gets there. Indeed, our observation that GalNAc

544 induces increased vesiculation provides evidence that either BT1927 is being lost from
545 the surface, or its protective effects are disrupted by the vesiculation that occurs during
546 growth in GalNAc. These observations also suggests that the mechanism of reduced
547 ARB25 resistance during growth in GalNAc is not identical to the mechanism that
548 sometimes generates the BT1927-off population in cells grown in fructose, or else we
549 would expect the GalNAc population to stain more weakly and identical to the
550 BT1927:OFF^{F} strain.

551 We do not yet understand the mechanism by which BT1927 protects against
552 phage or, in previous work, against complement-mediated killing. Given the prominent
553 structural organization that is observed on the cell surface when this protein is highly
554 expressed, an obvious hypothesis is that it physically blocks access to either
555 complement deposition and pore formation or phage adsorption. Since the ARB25
556 surface receptor remains unknown, it also remains unclear how much of the bacterial
557 surface needs to be covered by BT1927 to protect the cell. Indeed, this might not be an
558 all-or-nothing event, but rather, higher percent surface coverage decreases the odds
559 that a phage will access its receptor and infect the cell. Such a phenomenon could
560 explain the higher plaquing rates and clearer plaques we observe with GalNAc-grown
561 cells as well as the “intermediate” growth we often observe in liquid cultures of
562 BT1927:ON grown in GalNAc or conditions containing both GalNAc and fructose that
563 neither achieves full growth or full lysis. In the latter case, growth of protected cells and
564 killing of unprotected cells may balance each other, leading to little positive or negative
565 change in cell numbers measured by absorbance. Future work to identify the ARB25
566 receptor will open avenues to begin exploring these potential mechanisms in more

567 detail, for example, by increasing or decreasing the amount of ARB25 receptor and
568 seeing how those changes influence killing during growth in fructose or GalNAc.
569 Our research supports a model of dynamic interactions between phages and
570 intestinal bacteria, which is influenced by the carbohydrates present in the gut. The
571 reduced effectiveness of resistance proteins like BT1927 in the presence of nutrients
572 like GalNAc and *O*-glycans may explain why *B. thetaiotaomicron* possesses so many
573 different strategies (*i.e*., other resistance strategies like capsules may be more effective
574 and therefore relied upon in these growth conditions). Nevertheless, the ability of a
575 phage to persist in the microbiome alongside its prey bacterium like *B. thetaiotaomicron*
576 has implications for what cellular states (*e.g*., which CPS and S-layers are expressed)
577 the resistant bacterial population adopts during selection in the presence of phage. Cell
578 surface features like CPS and S-layers have other interactions with environmental
579 features like the host immune system and fiber polysaccharides (36, 59, 62–64) and, as
580 shown here, are further influenced by the carbohydrates *B. thetaiotaomicron* utilizes.
581 With this complex set of interactions between phage, nutrients, bacteria and host in
582 mind, it is likely that the variable presence of phage within the microbiomes of
583 individuals has broader impacts on holobiont physiology that extend beyond just simple
584 survival of the bacteria that are targeted by phage.

585

Table 1: Bacterial strains and plasmids used in this study			
Strain	**Genotype**	**Features**	**Reference**
***Bacteroides thetaiotaomicron* VPI-5482 and derivatives**			
acapsular	*tdk*$^-$ Δ*cps1-8*	Strain lacking all CPS synthesis loci	(65)
acapsular S-layer ON	*tdk*$^-$ Δ*cps1-8* BT1927:ON	Strain lacking all CPS synthesis loci, S-layer promoter locked in the ON orientation	(27)
acapsular S-layer OFF	*tdk*$^-$ Δ*cps1-8* BT1927:OFF	Strain lacking all CPS synthesis loci, S-layer promoter locked in the OFF orientation	(27)
acapsular S-layer ON FLAG	*tdk*$^-$ Δ*cps1-8* BT1927:ON FLAG	Strain lacking all CPS synthesis loci, S-layer promoter locked in the ON orientation with the C-terminal FLAG epitope	This study
acapsular S-layer OFF FLAG	*tdk*$^-$ Δ*cps1-8* BT1927:OFF FLAG	Strain lacking all CPS synthesis loci, S-layer promoter locked in the OFF orientation with the C-terminal FLAG epitope	This study
Δ*BT1222* acapsular	*tdk*$^-$ Δ*cps1-8* BT1927:ON	Strain lacking all CPS synthesis loci, gene deletion of *BT1222*	This study
Δ*BT1222* acapsular S-layer ON	*tdk*$^-$ Δ*cps1-8* BT1927:ON Δ*BT1222*	Strain lacking all CPS synthesis loci, S-layer promoter locked in the ON orientation, gene deletion of *BT1222*	This study
Δ*BT1222* acapsular S-layer ON FLAG	*tdk*$^-$ Δ*cps1-8* BT1927:ON Δ*BT1222* FLAG	Strain lacking all CPS synthesis loci, S-layer promoter locked in the ON orientation with the C-terminal FLAG epitope and gene deletion of *BT1222*	This study
Δ*BT4338* acapsular	*tdk*$^-$ Δ*cps1-8* Δ*BT4338*	Strain lacking all CPS synthesis loci, gene deletion of *BT1222*	This study

Δ*BT4338* acapsular S-layer ON	*tdk*⁻ Δ*cps1-8* BT1927:ON Δ*BT4338*	Strain lacking all CPS synthesis loci, S-layer promoter locked in the ON orientation, gene deletion of *BT1222*	This study
Δ*BT4338* acapsular S-layer ON FLAG	*tdk*⁻ Δ*cps1-8* BT1927:ON Δ*BT4338* FLAG	Strain lacking all CPS synthesis loci, S-layer promoter locked in the ON orientation with the C-terminal FLAG epitope and gene deletion of *BT1222*	This study
Plasmids in Escherichia coli S17-1 λpir, used for generation of B. thetaiotaomicron gene deletions			
pExchange BT1927-ON		Lock on BT1927 promoter	(36)
pExchange BT1927-OFF		Lock off BT1927 promoter	(36)
pExchange BT1927- ON FLAG		Lock on BT1927 promoter with C-terminal FLAG epitope	(36)
pExchange BT1927- OFF FLAG		Lock off BT1927 promoter with C-terminal FLAG epitope	(36)
pExchange Δ*BT1222*		*BT1222* deletion construct	This study
pExchange Δ*BT4338*		*BT14338* deletion construct	This study

586

Table 2. Primers used in this study		
Primer	**Sequence (5' - 3')**	**Use**
BT1502F	CATATTTTACAACGCCATCTTCACCAAC	BT1502 qPCR
BT1502R	CCGATGACAAAGGTAATAAACAGACTAAGA	BT1502 qPCR
BT1507F	CAGCCGGAACGAATGACTTACC	BT1507 qPCR
BT1507R	TGGATGTGATGAGGCTGATGCTAT	BT1507 qPCR
BT1512F	CGCCAACAATCTCAACCAACTTACT	BT1512 qPCR
BT1512R	TTTGGCGACTGCTAGCTATCATTTC	BT1512 qPCR
BT1792F	GAAACGGTTACGGAGAGCACTGAC	BT1792 qPCR
BT1792R	GGAAAACTATACCGAAGAAAACTACCTGA	BT1792 qPCR
BT1826F	TAGCAGCAGAAACCGGAGAAACA	BT1826 qPCR
BT1826R	ATGATGGTGAAATTGCAGATATAAAGAAAC	BT1826 qPCR
BT1927F	TCGCCTTTTTCAGATCAGTAGTTGG	BT1927 qPCR
BT1927R	ACGAAAATGGAGTTGAATGGAATAAGTT	BT1927 qPCR

BT2486F	AGCCTGGCGCCCGATAGA	BT2486 qPCR
BT2486R	CACAGGCTTTGACGCAGATGAA	BT2486 qPCR
BT4480F	GTGAAGATCGAATTTGGTGTGACG	BT4480 qPCR
BT4480R	ACGGATGAATTGCTCTGTGATAGTGTA	BT4480 qPCR
16SF	GGTAGTCCACACAGTAAACGATGAA	16S qPCR for normalization
16SR	CCCGTCAATTCCTTTGAGTTTC	16S qPCR for normalization
BT1222-5UP-SalI	GCGGTCGACCAATGGAATACTGAAAGACGAGCAGGAAG	BT1222 deletion construct
BT1222-3OUT	CATATCTTATATATTTTAAAATATTGTTTATGTAAGAAACACTTG	BT1222 deletion construct
BT1222-5OUT	CAAGTGTTTCTTACATAAACAATATTTTAAAATATATAAGATATGTGAGTACTTTTCTTTTGCCTTGATGCAAAA	BT1222 deletion construct
BT1222-3DWN-XbaI	GCGTCTAGAGCAAAGGCACCACCCCATACAGCG	BT1222 deletion construct
BT4338-5UP-SalI	GCGGTCGACCCATCATCGCTTCCGAAGCCATC	BT14338 deletion construct
BT4338-5IN	GGGTGCTACAAAACTGTGTTATACAGC	BT14338 deletion construct
BT4338-3IN	GCTGTATAACACAGTTTTGTAGCACCCTACAGACCTTATACGATCATAAAAAGTGATC	BT14338 deletion construct
BT4338-3DWN-XbaI	CCCTGATCGTCCGTCAGATGCCAGTG	BT14338 deletion construct

587

588 **Materials and Methods**

589 **Bacterial growth curves with phage**

590 Table 1 provides a list of strains used in this study. All *B. thetaiotaomicron*
591 cultures were grown in an anaerobic chamber (Coy Labs; 85% N2, 10% H2, 5% CO2)
592 at 37°C. In general, growth experiments were initiated by streaking freezer stocks
593 (cryopreserved in 25% final w/v glycerol) on *Bacteroides* phage recovery medium
594 (BPRM) agar with glucose as the main carbon source (66). High titer phage stocks
595 were propagated as previously described (27, 67). Briefly, the acapsular *B.*
596 *thetaiotaomicron* strain was incubated with 10ul of high titer phage for 20 min and plated
597 using a soft agar overlay, flooded after overnight incubation using sterile phage buffer
598 (100 mM NaCl, 8 mM MgSO4, 50 mM Tris pH 7.5, and 0.002% (w/v) gelatin), filter
599 sterilized, and the resulting phage titer determined using the acapsular strain as the
600 host.

601 Individual colonies of each strain were picked from BPRM agar after 3 days and
602 grown overnight in liquid BPRM medium with glucose as the main carbon source,
603 unless otherwise indicated. For growth experiments, an aliquot of each overnight culture
604 was centrifuged and washed twice with a 2X concentrated BPRM without any glucose
605 or other carbon source (BPRM no carbon). The washed cells were resuspended in
606 BPRM no carbon and 50ul was added to a 96-well microtiter plate wells containing
607 10mg/ml of carbohydrate as indicated in each growth curve, for a final concentration of
608 5mg/ml. 10ul of $5x10^6$ pfu/ml stock of either heat-killed (95°C for 30 min) or viable
609 phage was added to each well. Microtiter plates were covered with a gas-permeable,
610 optically clear membrane (Diversified Biotech), and optical density measured at 600nm

611 (OD_{600}) for 24-96 hours using a BioTek Synergy HT plate-reader connected to a
612 BioStack automated plate stacking device.
613
614 **Construction of *B. thetaiotaomicron* mutants**
615 All of the *B. thetaiotaomicron* mutants were created in the acapsular *B.*
616 *thetaiotaomicron (*Δcps Δtdk) strain, a mutant for thymidine kinase used to generate
617 allelic exchange mutants (68) and lacks all capsule. *B. thetaiotaomicron* Δcps
618 BT1927:ON and Δcps BT1927:OFF mutants were created from the previously
619 constructed BT1927-ON and BT1927-OFF strains (36) and the corresponding epitope
620 FLAG tagged constructs for each. The *BT1222* and *BT4338* gene deletion mutants
621 were generated by homologous regions for allelic exchange (68) with primers indicated
622 in Table 2. All mutants were confirmed by PCR and Sanger sequencing.
623
624 **Plaque Assay**
625 Isolated colonies of the BT1927:ON strain were cultured overnight in liquid
626 BPRM media and added to soft agar overlay as previously described (27) containing
627 either glucose, fructose or GalNAc as indicated. High titer ARB25 stocks were diluted
628 1:10 in series and 1ul was added to the soft agar containing the BT1927:ON or Δcps
629 strain, incubated overnight anaerobically, and quantified. To document plaque
630 morphology, images were captured using the GelDoc Go Gel Imaging System (Bio-Rad)
631 using a 0.8 sec exposure.
632
633

634 **Complement Survival Assay**

635 *B. thetaiotaomicron* strains were cultured overnight as described above from
636 isolated colonies in liquid BPRM media containing glucose. Cultures were prepared as
637 previously described (36). Briefly, Cells were centrifuged and washed once with PBS
638 and resuspended at 5×10^6 cells/ml in PBS supplemented with 0.5 mM MgCl2 and 1
639 mM CaCl2. Either 20% Human Serum or heat-inactivated human serum (56ºC for 30
640 min) was incubated with cells anaerobically at 37ºC for 1 hour. Cells were diluted in
641 series 1:10 and plated on BHI plates containing 10% horse blood anaerobically for 2
642 days. The percent survival of each strain was calculated by dividing the average
643 number of colonies from human serum vs heat-inactivated serum plates.

644

645 **RNA isolation and quantitative PCR (qPCR)**

646 To measure BT1927 and other gene transcript levels, cultures were grown as
647 described above in BPRM containing the different sugars indicated until they reached
648 OD_{600} between 0.5-0.6. Bacteria were collected by centrifugation (7,700xg for 2.5 min),
649 medium supernatants were removed, and pellets were resuspended in 500uL of
650 RNAprotect (Qiagen). RNA was extracted using RNeasy kit (Qiagen) and treated with
651 DNase I (NEB). cDNA was prepared using 1ug RNA via Superscript III Reverse
652 Transcriptase according to the manufacturer's instructions. qPCR analyses were
653 performed using a BioRad thermocycler and homemade qPCR Master Mix containing
654 SYBR green DNA dye (27) containing 500nM of BT1927 specific primers or 65nM 16S
655 rRNA primers (indicated in table 2) and 10ng cDNA. Amplification was performed for 40
656 cycles of 95ºC for 3 seconds, 55ºC for 20 seconds, and 72ºC for 8 seconds.

657 Normalization was performed using the 16S rRNA amplification and gene expression
658 between conditions was calculated using the DD cycle threshold (DDCt) method (69)
659 using the Δ*cps* strain, which expresses little *BT1927* in the absence of phage, as a
660 reference.
661
662 **Flow cytometry**
663 The *B. thetaiotaomicron* strain containing a FLAG epitope-tagged BT1927
664 locked-on strain was previously constructed (36) using the FLAG epitope tag to BT1927
665 C-terminus. Various strains containing this tagged allele were cultured as described
666 above with the addition of indicated carbohydrates and grown to OD_{600} between 0.5-0.6.
667 One milliliter of culture was centrifuged for 2 min in a microcentrifuge at 6,000 x g,
668 washed twice with PBS, and resuspended to approximately $5x10^6$ cells/ml in Bacteria
669 Staining buffer (BSB; 1% bovine serum albumin– 0.025% sodium azide–PBS, 0.5%
670 formaldehyde) and resuspended in BSB containing anti-FLAG Alexa Fluor 647-
671 conjugated antibody (1:25, Cell Signaling) and incubated for 1h at 37°C. Cells were
672 washed twice with BSB and were counterstained with SYTO BC Bacteria Stain
673 (Molecular Probes) and analyzed on an LSR Fortessa flow cytometer (BD). To minimize
674 carryover of cells, 3 blank samples of PBS were run between samples. Forward scatter
675 (FSC) and side scatter (SSC) data were set to logarithmic scale. After data acquisition,
676 *B. thetaiotaomicron* population was visualized on an allophycocyanin (APC-A)-
677 histogram plot using FlowJo software.
678
679

680 **Immunoblotting**

681 *B. thetaiotaomicron* strains containing the FLAG epitope-tagged BT1927 allele
682 (36) were cultured as described above with the addition of indicated carbohydrates and
683 grown to OD_{600} between 0.5-0.6. Samples were diluted 1:4 in Laemmli sample buffer
684 (Bio-Rad), heated for 10 min at 98°C and were run on a 4-12% Bis-Tris NuPAGE gel
685 (Invitrogen) and transferred onto a polyvinylidene difluoride membrane (0.2 µm) for
686 Western blot analysis. Membranes were blocked using Tris-buffered saline tween
687 (TBST)-based blocking solution (1M Tris, 5M NaCl, Tween 20) containing 5% milk,
688 stained with the anti-FLAG rabbit polyclonal primary antibody (1:1000, Cell Signaling),
689 washed twice with TBST, and goat polyclonal anti-rabbit (ThermoFisher) conjugated
690 Alexa Fluor 488 secondary antibody (1:1000). Imaging was performed using an
691 Odyssey CLx scanner (LI-COR).

692

693 **Proteomics**

694 The BT1927 locked-on strain was grown in BPRM containing either fructose or
695 GalNAc to OD_{600} between 0.5-0.6., cells were centrifuged (7,700xg for 2.5 min), washed
696 in PBS and frozen at -80°C. Cell pellets were resuspended in 500µl lysis buffer (4%
697 SDS, 50mM Tris, 10mM DTT, pH8.5), heated to 95°C for 10 min, cooled to room
698 temperature, and centrifuged for 2 min at 4,000 x g to remove cell debris and unlyzed
699 cells. Ice-cold acetone was added at 4:1 ratio and precipitated overnight at -20°C.
700 Proteins were centrifuged for 10 min at 4,000 x g, and the resulting pellets were washed
701 in 80% acetone before centrifuging at 17,000 x g for 10 min at 4°C. Supernatants were
702 removed, and the protein pellet allowed to air dry before resuspension in 75µl of

703 proteomics buffer (8M Urea, 50mM HEPES, pH8). Cell lystes were run on a 4-12% Bis-
704 Tris NuPAGE gel (Invitrogen) and subjected to Coomassie staining (Abcam).
705 Proteomics analysis was performed at the University of Michigan Proteomics Resource
706 Facility (PRF) using high-resolution LC-MS/MS, following a protocol refined by PRF as
707 previously described (70). The updated protocol included the following changes:
708 cysteines were alkylated with 65 mM 2-chloroacetamide; trypsin digestion occurred after
709 urea was diluted to <1.2 M, utilizing 0.5 µg of trypsin (Promega); and processed
710 peptides were reconstituted in 20 µL of Buffer A (100 mM NaOH). Peptides were
711 separated by liquid chromatography over 90 minutes in 2%–25% Buffer B (100 mM
712 NaOH and 500 mM sodium acetate) in 45 minutes, 25%–40% in 5 minutes, and 40%–
713 90% in 5 minutes, followed by holding at 90% buffer B for 5 minutes and equilibrating
714 with buffer A for 30 minutes). Proteins were identified by comparing the resulting tandem
715 mass spectrometry data against a database of all protein sequences in *B.*
716 *thetaiotaomicron* strain VPI-5482 (71). The parameters used were consistent with those
717 stated previously, except for a fragment tolerance of 0.1 kDa. The relative abundance of
718 each detected protein was determined based on MS1 abundances. Raw data is
719 available via the Proteomics Identifications Database (PRIDE) # PXD063111.
720
721 **Scanning Electron Microscopy**
722 For SEM imaging performed in Tuebingen, the BT1927:ON and BT1927:OFF
723 strains were grown on BHIS plates with 10% defibrinated sheep blood and grown
724 anaerobically for 4 days at 37°C. Individual colonies were picked into liquid BHIS
725 medium and grown for 15 hours at 37°C prior to fixation in 2.5% glutaraldehyde/4%

726 formaldehyde in PBS for 2 hours at room temperature. Sample processing and imaging
727 was performed by the Electron Microscopy Core at the Max Planck Institute for Biology
728 in Tübingen, Germany. Cells were mounted on poly-L-lysine-coated cover slips and
729 post-fixed with 1% osmium tetroxide for 45 minutes on ice. Subsequently, samples were
730 dehydrated in a graded ethanol series followed by critical point drying (CPD300, Leica
731 Microsystems) with CO_2. Finally, the cells were sputter-coated with a 3 nm thick layer of
732 platinum (CCU-010, Safematic) and examined with a field emission scanning electron
733 microscope (Regulus 8230, Hitachi High Technologies) at an accelerating voltage of 3
734 kV.

735 For Cell and OMV imaging at the University of Michigan, 3-day aged colonies of
736 the BT1927 locked-on strain were cultured in BPRM glucose for 20 hours and diluted
737 1:100 in BPRM containing either fructose or GalNAc to OD_{600} between 0.5-0.6, fixed in
738 2.5% glutaraldehyde/4% formaldehyde in PBS for 2 hours at room temperature,
739 mounted on poly-L-lysine-coated cover slips, and post-fixed with 1% osmium tetroxide
740 for 45 minutes on ice. Samples were dehydrated in a graded ethanol series followed by
741 critical point drying (CPD300, Leica Microsystems) with CO_2 and sputter coated 3 nm
742 thick layer of gold and examined with a field emission scanning electron microscope
743 (Thermo Fisher Nova 200 Nanolab SEM/FIB) at an accelerating voltage of 3 kV. OMV
744 particles were quantified by normalized image size, creation of 10x10mm boxes almost
745 devoid of cells, images were blinded and OMV particles were quantified. OMV particle
746 count was divided by the total area to account for any differences in the number of
747 boxes per image.
748

Acknowledgments

We acknowledge support from the University of Michigan Biomedical Research Core Facilities (Proteomics Resource Facility and Microscopy core), which is supported by a National Institutes of Health (NIH) Center Grant (University of Michigan Center for Gastrointestinal Research, P30 DK034933). J.J.F was supported by funds from the NIH T32 Genetics Training Program (T32GM007544) and the Howard Hughes Medical Institute Gilliam Fellowship (GT15133) for which we are extremely grateful. We acknowledge the Electron Microscopy Core Facility at the Max Planck Institute for Biology Tuebingen, especially Jürgen Berger and Katharina Hipp, for their expertise and support from the Max Planck Society to SLH and REL. We acknowledge the financial support of the University of Michigan College of Engineering, NSF grant (DMR-0320740), and technical support from the Michigan Center for Materials Characterization.

763 **Figure Legends**

764 **Figure 1. Colony aging increases BT1927-mediated resistance to ARB25 phage.**
765 (**A**) Growth of unaged (red), aged (green) BT1927:ON strain or BT1927:OFF (blue)
766 grown in media containing glucose and challenged with viable ARB25 or heat-killed
767 (HK) ARB25 (black curves). (**B**) Maximum absorbance differences of HK ARB25
768 (uninfected) versus ARB25 challenged unaged or aged BT1927:ON or BT1927:OFF
769 strain, calculated at 24-hours (One way ANOVA, **** P<0.0001, *** P=0.0009).

770

771 **Figure 2. BT1927 expression is associated with a crystalline surface structure.**
772 SEM images of the BT1927:OFF strain (**A**) or BT1927:ON strain (**B**). (**C**) Multiple cells
773 of the BT1927:ON strain showing the presence of both coated and uncoated cells.
774 Enlarged inlaid images are provided for each panel to highlight presence or absence of
775 structural features and uncoated or coated cells.

776

777 **Figure 3. Different carbohydrates modify susceptibility to ARB25 phage.** (**A**)
778 Growth of the unaged BT1927:ON strain treated with viable ARB25 (red) or HK ARB25
779 (black), passaged for 5 days in glucose. (**B**) Growth of the BT1927:ON strain in media
780 containing Fructose (**C**) Growth of the BT1927:ON strain in media containing GalNAc.
781 The delta symbol in C and D indicates the absorbance difference measured to quantify
782 growth differences between ARB25 and HK. (**D**) Ranked monosaccharide results in
783 order of higher to lower ARB25 susceptibility. (**E**) Ranked polysaccharide results in order
784 of higher to lower ARB25 susceptibility.

785

786 **Figure 4. GalNAc increases susceptibility to ARB25 phage.** (**A**) Maximum
787 absorbance differences from passaged growth experiments for 5-days in medium
788 containing glucose (black), fructose (blue), GalNAc (red), or a 1:1 mixture of fructose
789 and GalNAc (orange) at 5mg/ml each, n = 3 per condition (One way ANOVA, ****
790 P<0.0001, *** P=0.0002, ** P<0.005, *P<0.05). (**B**) Quantification of plaque forming
791 units with indicated strains grown in top agar containing fructose (blue) or GalNAc (red)
792 compared to the more susceptible acapsular control (Δcps; black), n = 3 per condition,
793 (one-tailed t-test, **P=0.0066). (**C**) Representative images of plaques formed under the
794 indicated conditions and strains as depicted in B.
795
796 **Figure 5. BT1927 surface protein abundance is modified by GalNAc.** (**A**) Flow
797 cytometry histograms for BT1927 expression indicated by intensity of FLAG epitope
798 staining (APC-A) in the BT1927:OFF^F (grey) strain grown in fructose or the BT1927:ON^F
799 strain grown in medium with either fructose (blue) or GalNAc (red). (**B**) Same conditions
800 as depicted in A but with the addition of staining of cells grown in a mixture of GalNAc
801 and fructose (5mg/ml each; orange) instead of GalNAc only. The smaller plots at right
802 show the three individual plots of growth in fructose in which cell population (bottom)
803 displayed a sub-population of cells that stain similarly to the BT1927:OFF^F strain. (**C**)
804 BT1927 transcript expression in the BT1927:ON strain grown in either fructose (blue) or
805 GalNac (red). (**D**) Normalized protein abundance in BT1927:ON strain grown in fructose
806 (blue) or GalNac (red). (**E**) OMV particle count per mm^2 from cells grown in either
807 glucose (black), fructose (blue) or GalNAc (red) (Welch ANOVA, **** P<0.0001). (**F**)

808 representative images for each condition in E. Arrows indicate apparent OMV particles
809 either cell associated (white) or free from cells (black).
810
811 **Figure 6. Mutants in the oxidative branch of the pentose phosphate pathway**
812 **increase susceptibility to ARB25 phage.** (**A**) Growth of acapsular *B. thetaiotaomicron*
813 or a transposon mutant in this same strain with disrupted *BT1222* and treated with HK
814 ARB25 (black) or ARB25 (red). (**B**) Growth of the BT1927:ON strain (black) or a *BT1222*
815 deletion (grey) mutant in the BT1927:ON strain background and treated with HK ARB25
816 or ARB25 (red or dark red, respectively). (**C**) qPCR measurement of *BT1927* transcript
817 in the BT1927:ON strain (light blue) or BT1222 mutant (light red). (**D**) Histograms of
818 epitope-tagged BT1927 (APC-A) for either the BT1927:ON strain (blue) or BT1222
819 mutant (red) grown in fructose.
820
821 **Figure S1.** (**A**) SEM imaging of the BT1927:ON strain with cells that exhibit BT1927
822 associated crystalline coating over most of their surface (pink dot, green circle) and
823 what appear to be uncoated cells (green circle only). (**B**) Maximum absorbance (abs)
824 differences of unaged BT1927:ON after 5-days of passage in glucose and subsequent
825 passage into fructose or GalNAc. (**C**) Maximum absorbance (abs) differences of aged
826 BT1927:ON after 5-days of passage in glucose and subsequent passage into fructose
827 or GalNAc. (**D**) Growth of the BT1927:ON strain in BPRM medium containing the
828 carbohydrates listed above each graph as the sole carbohydrate source (5mg/ml, n= 3
829 per condition).
830

831 **Figure S2.** (**A**) Absorbance difference between ARB25 infected and HK control for
832 cultures grown in GalNAc, glucose, or fructose (One-way ANOVA, **** P<0.0001,
833 ***P=0.0002, **P<0.007, *P<0.05). (**B**) Cultures of the BT1927:ON strain grown in
834 fructose or GalNAc for RNA collection with harvest points indicated by red circles in the
835 infected and HK control for each curve. (**C**) Transcript expression measurements for
836 each phase-variable S-layer or other system as measured by qPCR in fructose and
837 GalNAc. (**D**) BT1927:ON cultures treated with HK *B. thetaiotaomicron* phage (black) or
838 challenged with the 6 indicated *B. thetaiotaomicron* phages in BPRM containing
839 fructose (top) GalNAc (middle) or mucin *O*-glycans (MOG; Bottom), n = 3 per condition.
840
841 **Figure S3.** (**A**) Growth of daily passaged BT1927:ON cultures in BPRM medium
842 containing glucose (5 days) and subsequent growth after passage into fructose,
843 GalNAc, or 1:1 mixture of fructose and GalNAc (at 5mg/ml each) as indicated, n = 3 per
844 condition. (**B**) ARB25 infection kinetics for BT1927:ON cultures grown on a solid
845 medium containing glucose, grown in liquid culture containing glucose and sub-cultured
846 again into liquid media containing GalNAc (as indicated above title) and challenged with
847 ARB25 phage. (**C**) ARB25 infection kinetics for BT1927:ON cultures grown on a solid
848 medium containing GalNAc, grown in liquid culture containing GalNAc and sub-cultured
849 again into liquid media containing GalNAc (as indicated above title) and challenged with
850 ARB25 phage. (**D**) Percent survival of BT1927:ON grown in either fructose (blue) or
851 GalNAc (red) or the BT1927:OFF strain grown in fructose (grey) challenged with pooled
852 human complement and normalized to the no complement control. (**E**) Growth of the

853 epitope tagged BT1927:ON^F strain treated with HKARB25 (black) or ARB25 (red)
854 demonstrating the FLAG tag does not inhibit BT1927-mediated resistance.
855
856 **Figure S4.** (**A**) Flow cytometry histogram for the BT1927:ON^F strain grown in BPRM
857 medium containing fructose or GalNAc from an experiment in which all 3 replicates
858 showed a BT1927 low staining population. (**B**) Flow cytometry histogram for the
859 BT1927:ON^F strain grown in BPRM medium containing fructose or GalNAc from an
860 experiment in which replicates were grown in different anaerobic chamber and one
861 showed a BT1927 low staining population. (**C**) *BT1927* transcript expression in the
862 BT1927:ON strain grown in glucose (black) or glucosamine (grey) at mid-log phase. (**D**)
863 Western blot of whole cells of the BT1927:ON^F strain grown in either fructose or GalNAc
864 and stained for BT1927-FLAG. (**E**) Normalized protein abundance for products of the
865 levan associated PUL that is known to be induced by fructose (two-tailed t-test, P
866 *<0.001, **<0.05, *** <0.005). (**F**) SEM images of the BT1927:ON strain grown in
867 fructose from which OMV measurements were made. (**G**) SEM images of the
868 BT1927:ON strain grown in GalNAc from which OMV measurements were made. In F
869 and G, boxes indicate normalized area used for blinded counting of OMV particles.
870
871 **Figure S5.** (**A-E**) Growth of the acapsular *B. thetaiotaomicron* strain (A) and transposon
872 mutants in the acpasular *B. thetaiotaomicron* with insertions in genes encoding the 3
873 steps of the oxidative branch of the pentose phosphate pathway and a linked genes
874 encoding a putative carboxylate transporter. In each panel, cultures were treated with
875 HK ARB25 (black) or ARB25 (red). (**F**) Quantification of plaques formed on the

876 BT1927:ON strain (blue), a *BT1222* deletion in the 1927:ON strain background (red) or
877 the susceptible acapsular strain (black). (**G**) Western blot of the BT1927:ON^F or
878 Δ*BT1222* mutant in the BT1927:ON^F strain as indicated above each column. (**H**)
879 Growth of the acapsular *B. thetaiotaomicron* or Δ*BT4338* deletion mutant strain in the
880 same acapsular background treated with HK ARB25 or ARB25 (red or dark red,
881 respectively). (**I**) Growth of the BT1927:ON (black) or corresponding Δ*BT4338* deletion
882 mutant in the same background (grey) in the BT1927:ON strain treated with HK ARB25
883 or ARB25 (red or dark red, respectively). (**J**) Histogram of staining for the epitope-
884 tagged BT1927 (APC-A) in either the BT1927:ON strain (blue) or a Δ*BT4338* mutant in
885 this same background (red), grown in fructose.
886

887 **References**

888 1. Glowacki RWP, Martens EC. 2021. If You Eat It or Secrete It, They Will Grow: the
889 Expanding List of Nutrients Utilized by Human Gut Bacteria. *Journal of*
890 *Bacteriology* 203: 10.1128/jb.00481-20.

891 2. Flint HJ, Bayer EA, Rincon MT, Lamed R, White BA. 2008. Polysaccharide utilization
892 by gut bacteria: potential for new insights from genomic analysis. *Nature Reviews*
893 *Microbiology* 6: 121–131.

894 3. Vasquez Ayala A, Hsu C-Y, Oles RE, Matsuo K, Loomis LR, Buzun E, Carrillo
895 Terrazas M, Gerner RR, Lu H-H, Kim S, Zhang Z, Park JH, Rivaud P, Thomson M,
896 Lu L-F, Min B, Chu H. 2023. Commensal bacteria promote type I interferon
897 signaling to maintain immune tolerance in mice. *Journal of Experimental Medicine*
898 221: e20230063.

899 4. Belkaid Y, Harrison OJ. 2017. Homeostatic Immunity and the Microbiota. *Immunity*
900 46: 562–576.

901 5. Mao K, Baptista AP, Tamoutounour S, Zhuang L, Bouladoux N, Martins AJ, Huang Y,
902 Gerner MY, Belkaid Y, Germain RN. 2018. Innate and adaptive lymphocytes
903 sequentially shape the gut microbiota and lipid metabolism. *Nature* 554: 255–259.

904 6. Lawley TD, Walker AW. 2013. Intestinal colonization resistance. *Immunology* 138:
905 1–11.

906 7. Li Z, Quan G, Jiang X, Yang Y, Ding X, Zhang D, Wang X, Hardwidge PR, Ren W,
907 Zhu G. 2018. Effects of Metabolites Derived From Gut Microbiota and Hosts on
908 Pathogens. *Frontiers in Cellular and Infection Microbiology* 8: 314.

909 8. David LA, Maurice CF, Carmody RN, Gootenberg DB, Button JE, Wolfe BE, Ling AV,
910 Devlin AS, Varma Y, Fischbach MA, Biddinger SB, Dutton RJ, Turnbaugh PJ. 2014.
911 Diet rapidly and reproducibly alters the human gut microbiome. *Nature* 505: 559–
912 563.

913 9. Faith JJ, Guruge JL, Charbonneau M, Subramanian S, Seedorf H, Goodman AL,
914 Clemente JC, Knight R, Heath AC, Leibel RL, Rosenbaum M, Gordon JI. 2013. The
915 Long-Term Stability of the Human Gut Microbiota. *Science* 341: 1237439.

916 10. Wastyk HC, Fragiadakis GK, Perelman D, Dahan D, Merrill BD, Yu FB, Topf M,
917 Gonzalez CG, Van Treuren W, Han S, Robinson JL, Elias JE, Sonnenburg ED,
918 Gardner CD, Sonnenburg JL. 2021. Gut-microbiota-targeted diets modulate human
919 immune status. *Cell* 184: 4137–4153.

920 11. Tropini C, Moss EL, Merrill BD, Ng KM, Higginbottom SK, Casavant EP, Gonzalez
921 CG, Fremin B, Bouley DM, Elias JE, Bhatt AS, Huang KC, Sonnenburg JL. 2018.
922 Transient Osmotic Perturbation Causes Long-Term Alteration to the Gut Microbiota.
923 *Cell* 173: 1742–1754.

924 12. Gogokhia L, Buhrke K, Bell R, Hoffman B, Brown DG, Hanke-Gogokhia C, Ajami
925 NJ, Wong MC, Ghazaryan A, Valentine JF, Porter N, Martens E, O'Connell R,
926 Jacob V, Scherl E, Crawford C, Stephens WZ, Casjens SR, Longman RS, Round

927 JL. 2019. Expansion of Bacteriophages Is Linked to Aggravated Intestinal
928 Inflammation and Colitis. *Cell Host & Microbe* 25: 285–299.

929 13. Carasso S, Zaatry R, Hajjo H, Kadosh-Kariti D, Ben-Assa N, Naddaf R,
930 Mandelbaum N, Pressman S, Chowers Y, Gefen T, Jeffrey KL, Jofre J, Coyne MJ,
931 Comstock LE, Sharon I, Geva-Zatorsky N. 2024. Inflammation and bacteriophages
932 affect DNA inversion states and functionality of the gut microbiota. *Cell Host &*
933 *Microbe* 32: 322–334.

934 14. Clooney AG, Sutton TDS, Shkoporov AN, Holohan RK, Daly KM, O'Regan O, Ryan
935 FJ, Draper LA, Plevy SE, Ross RP, Hill C. Whole-Virome Analysis Sheds Light on
936 Viral Dark Matter in Inflammatory Bowel Disease. *Cell Host & Microbe*
937 https://doi.org/10.1016/j.chom.2019.10.009.

938 15. Lourenço M, Chaffringeon L, Lamy-Besnier Q, Pédron T, Campagne P, Eberl C,
939 Bérard M, Stecher B, Debarbieux L, Sordi LD. 2020. The Spatial Heterogeneity of
940 the Gut Limits Predation and Fosters Coexistence of Bacteria and Bacteriophages.
941 *Cell Host & Microbe* 28: 390–401.

942 16. Tobin CA, Hill C, Shkoporov AN. 2023. Factors Affecting Variation of the Human
943 Gut Phageome. *Annual Review of Microbiology* 77: 363–379.

944 17. Huttenhower C, Gevers D, Knight R, Abubucker S, Badger JH, Chinwalla AT,
945 Creasy HH, Earl AM, FitzGerald MG, Fulton RS, Giglio MG, Hallsworth-Pepin K,
946 Lobos EA, Madupu R, Magrini V, Martin JC, Mitreva M, Muzny DM, Sodergren EJ,
947 Versalovic J, Wollam AM, Worley KC, Wortman JR, Young SK, Zeng Q, Aagaard

948 KM, Abolude OO, Allen-Vercoe E, Alm EJ, Alvarado L, Andersen GL, Anderson S,
949 Appelbaum E, Arachchi HM, Armitage G, Arze CA, Ayvaz T, Baker CC, Begg L,
950 Belachew T, Bhonagiri V, Bihan M, Blaser MJ, Bloom T, Bonazzi V, Paul Brooks J,
951 Buck GA, Buhay CJ, Busam DA, Campbell JL, Canon SR, Cantarel BL, Chain
952 PSG, Chen I-MA, Chen L, Chhibba S, Chu K, Ciulla DM, Clemente JC, Clifton SW,
953 Conlan S, Crabtree J, Cutting MA, Davidovics NJ, Davis CC, DeSantis TZ, Deal C,
954 Delehaunty KD, Dewhirst FE, Deych E, Ding Y, Dooling DJ, Dugan SP, Michael
955 Dunne W, Scott Durkin A, Edgar RC, Erlich RL, Farmer CN, Farrell RM, Faust K,
956 Feldgarden M, Felix VM, Fisher S, Fodor AA, Forney LJ, Foster L, Di Francesco V,
957 Friedman J, Friedrich DC, Fronick CC, Fulton LL, Gao H, Garcia N, Giannoukos G,
958 Giblin C, Giovanni MY, Goldberg JM, Goll J, Gonzalez A, Griggs A, Gujja S, Kinder
959 Haake S, Haas BJ, Hamilton HA, Harris EL, Hepburn TA, Herter B, Hoffmann DE,
960 Holder ME, Howarth C, Huang KH, Huse SM, Izard J, Jansson JK, Jiang H, Jordan
961 C, Joshi V, Katancik JA, Keitel WA, Kelley ST, Kells C, King NB, Knights D, Kong
962 HH, Koren O, Koren S, Kota KC, Kovar CL, Kyrpides NC, La Rosa PS, Lee SL,
963 Lemon KP, Lennon N, Lewis CM, Lewis L, Ley RE, Li K, Liolios K, Liu B, Liu Y, Lo
964 C-C, Lozupone CA, Dwayne Lunsford R, Madden T, Mahurkar AA, Mannon PJ,
965 Mardis ER, Markowitz VM, Mavromatis K, McCorrison JM, McDonald D, McEwen
966 J, McGuire AL, McInnes P, Mehta T, Mihindukulasuriya KA, Miller JR, Minx PJ,
967 Newsham I, Nusbaum C, O'Laughlin M, Orvis J, Pagani I, Palaniappan K, Patel
968 SM, Pearson M, Peterson J, Podar M, Pohl C, Pollard KS, Pop M, Priest ME,
969 Proctor LM, Qin X, Raes J, Ravel J, Reid JG, Rho M, Rhodes R, Riehle KP, Rivera
970 MC, Rodriguez-Mueller B, Rogers Y-H, Ross MC, Russ C, Sanka RK, Sankar P,

971 Fah Sathirapongsasuti J, Schloss JA, Schloss PD, Schmidt TM, Scholz M, Schriml
972 L, Schubert AM, Segata N, Segre JA, Shannon WD, Sharp RR, Sharpton TJ,
973 Shenoy N, Sheth NU, Simone GA, Singh I, Smillie CS, Sobel JD, Sommer DD,
974 Spicer P, Sutton GG, Sykes SM, Tabbaa DG, Thiagarajan M, Tomlinson CM,
975 Torralba M, Treangen TJ, Truty RM, Vishnivetskaya TA, Walker J, Wang L, Wang Z,
976 Ward DV, Warren W, Watson MA, Wellington C, Wetterstrand KA, White JR,
977 Wilczek-Boney K, Wu Y, Wylie KM, Wylie T, Yandava C, Ye L, Ye Y, Yooseph S,
978 Youmans BP, Zhang L, Zhou Y, Zhu Y, Zoloth L, Zucker JD, Birren BW, Gibbs RA,
979 Highlander SK, Methé BA, Nelson KE, Petrosino JF, Weinstock GM, Wilson RK,
980 White O, The Human Microbiome Project Consortium. 2012. Structure, function
981 and diversity of the healthy human microbiome. *Nature* 486: 207–214.

982 18. Mehta RS, Abu-Ali GS, Drew, David A., Lloyd-Price, Jason, Subramanian,
983 Ayshwarya, Lochhead, Paul, Joshi, Amit D., Ivey, Kerry L., Khalili, Hamed, Brown,
984 Gordon T., DuLong, Casey, Song, Mingyang, Nguyen, Long H., Mallick, Himel,
985 Rimm, Eric B., Izard, Jacques, Huttenhower, Curtis, Chan, Andrew T. 2018.
986 Stability of the human faecal microbiome in a cohort of adult men. *Nature*
987 *Microbiology* 3: 347–355.

988 19. Reyes A, Wu M, McNulty NP, Rohwer FL, Gordon JI. 2013. Gnotobiotic mouse
989 model of phage-bacterial host dynamics in the human gut. *Proceedings of the*
990 *National Academy of Sciences* 110: 20236–20241.

991 20. Rasmussen TS, Koefoed AK, Deng L, Muhammed MK, Rousseau GM, Kot W,
992 Sprotte S, Neve H, Franz CMAP, Hansen AK, Vogensen FK, Moineau S, Nielsen

993 DS. 2023. CRISPR-Cas provides limited phage immunity to a prevalent gut
994 bacterium in gnotobiotic mice. *The ISME Journal* 17: 432–442.

995 21. Jackson SA, McKenzie RE, Fagerlund RD, Kieper SN, Fineran PC, Brouns SJJ.
996 2017. CRISPR-Cas: Adapting to change. *Science* 356: eaal5056.

997 22. Beavogui A, Lacroix A, Wiart N, Poulain J, Delmont TO, Paoli L, Wincker P, Oliveira
998 PH. 2024. The defensome of complex bacterial communities. *Nature*
999 *Communications* 15: 2146.

1000 23. Whiteley AT, Eaglesham JB, de Oliveira Mann CC, Morehouse BR, Lowey B,
1001 Nieminen EA, Danilchanka O, King DS, Lee ASY, Mekalanos JJ, Kranzusch PJ.
1002 2019. Bacterial cGAS-like enzymes synthesize diverse nucleotide signals. *Nature*
1003 567: 194–199.

1004 24. Lowey B, Whiteley AT, Keszei AFA, Morehouse BR, Mathews IT, Antine SP,
1005 Cabrera VJ, Kashin D, Niemann P, Jain M, Schwede F, Mekalanos JJ, Shao S, Lee
1006 ASY, Kranzusch PJ. 2020. CBASS Immunity Uses CARF-Related Effectors to
1007 Sense 3′–5′- and 2′–5′-Linked Cyclic Oligonucleotide Signals and Protect Bacteria
1008 from Phage Infection. *Cell* 182: 38-49.e17.

1009 25. O'Neill M, Chen A, Murray NE. 1997. The restriction–modification genes of
1010 *Escherichia coli* K-12 may not be selfish: They do not resist loss and are readily
1011 replaced by alleles conferring different specificities. *Proceedings of the National*
1012 *Academy of Sciences of the United States of America* 94: 14596–14601.

1013 26. Vassallo CN, Doering CR, Littlehale ML, Teodoro GIC, Laub MT. 2022. A functional
1014 selection reveals previously undetected anti-phage defence systems in the *E. coli*
1015 pangenome. *Nature Microbiology* 7: 1568–1579.

1016 27. Porter NT, Hryckowian AJ, Merrill BD, Fuentes JJ, Gardner JO, Glowacki RWP,
1017 Singh S, Crawford RD, Snitkin ES, Sonnenburg JL, Martens EC. 2020. Phase-
1018 variable capsular polysaccharides and lipoproteins modify bacteriophage
1019 susceptibility in *Bacteroides thetaiotaomicron. Nature Microbiology* 5: 1170–1181.

1020 28. Shkoporov AN, Khokhlova EV, Stephens N, Hueston C, Seymour S, Hryckowian
1021 AJ, Scholz D, Ross RP, Hill C. 2021. Long-term persistence of crAss-like phage
1022 crAss001 is associated with phase variation in *Bacteroides intestinalis. BMC*
1023 *Biology* 19: 163.

1024 29. Shkoporov AN, Hill C. 2019. Bacteriophages of the Human Gut: The “Known
1025 Unknown” of the Microbiome. *Cell Host & Microbe* 25: 195–209.

1026 30. Booth SJ, Van Tassell RL, Johnson JL, Wilkins TD. 1979. Bacteriophages of
1027 *Bacteroides. Reviews of Infectious Diseases* 1: 325–336.

1028 31. Keller R, Traub N. 1974. The characterization of *Bacteroides fragilis* bacteriophage
1029 recovered from animal sera: observations on the nature of bacteroides phage
1030 carrier cultures. *The Journal of General Virology* 24: 179–189.

1031 32. Shkoporov AN, Clooney AG, Sutton TDS, Ryan FJ, Daly KM, Nolan JA, McDonnell
1032 SA, Khokhlova EV, Draper LA, Forde A, Guerin E, Velayudhan V, Ross RP, Hill C.

1033 2019. The Human Gut Virome Is Highly Diverse, Stable, and Individual Specific.
1034 *Cell Host & Microbe* 26: 527–541.

1035 33. Norman JM, Handley SA, Baldridge MT, Droit L, Liu CY, Keller BC, Kambal A,
1036 Monaco CL, Zhao G, Fleshner P, Stappenbeck TS, McGovern DP, Keshavarzian A,
1037 Mutlu EA, Sauk J, Gevers D, Xavier RJ, Wang D, Parkes M, Virgin HW. 2015.
1038 Disease-specific alterations in the enteric virome in inflammatory bowel disease.
1039 *Cell*, 2015/01/27 ed. 160: 447–60.

1040 34. Fagan RP, Fairweather NF. 2014. Biogenesis and functions of bacterial S-layers.
1041 *Nature Reviews Microbiology* 12: 211–222.

1042 35. Sleytr UB, Beveridge TJ. 1999. Bacterial S-layers. *Trends in Microbiology* 7: 253–
1043 260.

1044 36. Taketani M, Donia MS, Jacobson AN, Lambris JD, Fischbach MA. 2015. A Phase-
1045 Variable Surface Layer from the Gut Symbiont *Bacteroides thetaiotaomicron. mBio*
1046 6: 10.1128/mbio.01339-15.

1047 37. Cuskin F, Lowe EC, Temple MJ, Zhu Y, Cameron EA, Pudlo NA, Porter NT, Urs K,
1048 Thompson AJ, Cartmell A, Rogowski A, Hamilton BS, Chen R, Tolbert TJ, Piens K,
1049 Bracke D, Vervecken W, Hakki Z, Speciale G, Munōz-Munōz JL, Day A, Peña MJ,
1050 McLean R, Suits MD, Boraston AB, Atherly T, Ziemer CJ, Williams SJ, Davies GJ,
1051 Abbott DW, Martens EC, Gilbert HJ. 2015. Human gut Bacteroidetes can utilize
1052 yeast mannan through a selfish mechanism. *Nature* 517: 165–169.

1053 38. Larsbrink J, Rogers TE, Hemsworth GR, McKee LS, Tauzin AS, Spadiut O, Klinter
1054 S, Pudlo NA, Urs K, Koropatkin NM, Creagh AL, Haynes CA, Kelly AG, Cederholm
1055 SN, Davies GJ, Martens EC, Brumer H. 2014. A discrete genetic locus confers
1056 xyloglucan metabolism in select human gut Bacteroidetes. *Nature* 506: 498–502.

1057 39. Martens EC, Chiang HC, Gordon JI. 2008. Mucosal Glycan Foraging Enhances
1058 Fitness and Transmission of a Saccharolytic Human Gut Bacterial Symbiont. *Cell*
1059 *Host & Microbe* 4: 447–457.

1060 40. Cockburn DW, Koropatkin NM. 2016. Polysaccharide Degradation by the Intestinal
1061 Microbiota and Its Influence on Human Health and Disease. *Journal of molecular*
1062 *biology*, 2016/07/10 ed. 428: 3230–3252.

1063 41. Bjursell MK, Martens EC, Gordon JI. 2006. Functional Genomic and Metabolic
1064 Studies of the Adaptations of a Prominent Adult Human Gut Symbiont, *Bacteroides*
1065 *thetaiotaomicron*, to the Suckling Period. *Journal of Biological Chemistry* 281:
1066 36269–36279.

1067 42. Chatterjee S, Rothenberg E. 2012. Interaction of Bacteriophage λ with Its *E. coli*
1068 Receptor, LamB. *Viruses* 4: 3162–3178.

1069 43. Bonhivers M, Plançon L, Ghazi A, Boulanger A, le Maire M, Lambert O, Rigaud JL,
1070 Letellier L. 1998. FhuA, an *Escherichia coli* outer membrane protein with a dual
1071 function of transporter and channel which mediates the transport of phage DNA.
1072 *Biochimie* 80: 363–369.

1073 44. Sonnenburg ED, Zheng H, Joglekar P, Higginbottom SK, Firbank SJ, Bolam DN,
1074 Sonnenburg JL. 2010. Specificity of Polysaccharide Use in Intestinal Bacteroides
1075 Species Determines Diet-Induced Microbiota Alterations. *Cell* 141: 1241–1252.

1076 45. Sartorio MG, Pardue EJ, Scott NE, Feldman MF. 2023. Human gut bacteria tailor
1077 extracellular vesicle cargo for the breakdown of diet- and host-derived glycans.
1078 *Proceedings of the National Academy of Sciences* 120: e2306314120.

1079 46. Engelhart MJ, Glowacki RWP, Till JM, Harding CV, Martens EC, Ahern PP. 2023.
1080 The NQR Complex Regulates the Immunomodulatory Function of *Bacteroides*
1081 *thetaiotaomicron. The Journal of Immunology* 211: 767–781.

1082 47. Pardue EJ, Sartorio MG, Jana B, Scott NE, Beatty WL, Ortiz-Marquez JC, Van
1083 Opijnen T, Hsu F-F, Potter RF, Feldman MF. 2024. Dual membrane-spanning anti-
1084 sigma factors regulate vesiculation in *Bacteroides thetaiotaomicron. Proceedings of*
1085 *the National Academy of Sciences* 121: e2321910121.

1086 48. Martens EC, Lowe EC, Chiang H, Pudlo NA, Wu M, McNulty NP, Abbott DW,
1087 Henrissat B, Gilbert HJ, Bolam DN, Gordon JI. 2011. Recognition and Degradation
1088 of Plant Cell Wall Polysaccharides by Two Human Gut Symbionts. *PLoS Biology* 9:
1089 e1001221.

1090 49. Pudlo NA, Urs K, Kumar SS, German JB, Mills DA, Martens EC. 2015. Symbiotic
1091 Human Gut Bacteria with Variable Metabolic Priorities for Host Mucosal Glycans.
1092 *mBio* 6: 10.1128/mbio.01282-15.

1093 50. Pearce VH, Groisman EA, Townsend GE. 2023. Dietary sugars silence the master
1094 regulator of carbohydrate utilization in human gut *Bacteroides* species. *Gut*
1095 *Microbes* 15: 2221484.

1096 51. Wegorzewska MM, Glowacki RWP, Hsieh SA, Donermeyer DL, Hickey CA, Horvath
1097 SC, Martens EC, Stappenbeck TS, Allen PM. 2019. Diet modulates colonic T cell
1098 responses by regulating the expression of a *Bacteroides thetaiotaomicron* antigen.
1099 *Science Immunology* 4: eaau9079.

1100 52. Liou CS, Sirk SJ, Diaz CAC, Klein AP, Fischer CR, Higginbottom SK, Erez A, Donia
1101 MS, Sonnenburg JL, Sattely ES. 2020. A Metabolic Pathway for Activation of
1102 Dietary Glucosinolates by a Human Gut Symbiont. *Cell* 180: 717–728.

1103 53. Dion MB, Oechslin F, Moineau S. 2020. Phage diversity, genomics and phylogeny.
1104 *Nature Reviews Microbiology* 18: 125–138.

1105 54. Townsend EM, Kelly L, Muscatt G, Box JD, Hargraves N, Lilley D, Jameson E.
1106 2021. The Human Gut Phageome: Origins and Roles in the Human Gut
1107 Microbiome. *Frontiers in Cellular and Infection Microbiology* 11.

1108 55. Schaus SR, Vasconcelos Pereira G, Luis AS, Madlambayan E, Terrapon N,
1109 Ostrowski MP, Jin C, Henrissat B, Hansson GC, Martens EC. 2024. *Ruminococcus*
1110 *torques* is a keystone degrader of intestinal mucin glycoprotein, releasing
1111 oligosaccharides used by *Bacteroides thetaiotaomicron. mBio* 15: e00039-24.

1112 56. Sonnenburg JL. 2005. Glycan Foraging in Vivo by an Intestine-Adapted Bacterial
1113 Symbiont. *Science* 307: 1955–1959.

1114 57. Earle KA, Billings G, Sigal M, Lichtman JS, Hansson GC, Elias JE, Amieva MR,
1115 Huang KC, Sonnenburg JL. 2015. Quantitative Imaging of Gut Microbiota Spatial
1116 Organization. *Cell Host & Microbe* 18: 478–488.

1117 58. Ben-Assa N, Coyne MJ, Fomenkov A, Livny J, Robins WP, Muniesa M, Carey V,
1118 Carasso S, Gefen T, Jofre J, Roberts RJ, Comstock LE, Geva-Zatorsky N. 2020.
1119 Analysis of a phase-variable restriction modification system of the human gut
1120 symbiont *Bacteroides fragilis. Nucleic Acids Research* 48: 11040–11053.

1121 59. Porter NT, Canales P, Peterson DA, Martens EC. 2017. A Subset of Polysaccharide
1122 Capsules in the Human Symbiont *Bacteroides thetaiotaomicron* Promote Increased
1123 Competitive Fitness in the Mouse Gut. *Cell Host & Microbe* 22: 494–506.

1124 60. Shkoporov AN, Khokhlova EV, Fitzgerald CB, Stockdale SR, Draper LA, Ross RP,
1125 Hill C. 2018. PhiCrAss001 represents the most abundant bacteriophage family in
1126 the human gut and infects *Bacteroides intestinalis. Nature communications*,
1127 2018/11/16 ed. 9: 4781.

1128 61. Chanin RB, West PT, Wirbel J, Gill MO, Green GZM, Park RM, Enright N, Miklos
1129 AM, Hickey AS, Brooks EF, Lum KK, Cristea IM, Bhatt AS. 2024. Intragenic DNA
1130 inversions expand bacterial coding capacity. *Nature* 634: 234–242.

1131 62. Chu H, Khosravi A, Kusumawardhani IP, Kwon AHK, Vasconcelos AC, Cunha LD,
1132 Mayer AE, Shen Y, Wu W-L, Kambal A, Targan SR, Xavier RJ, Ernst PB, Green
1133 DR, McGovern DPB, Virgin HW, Mazmanian SK. 2016. Gene-microbiota

1134 interactions contribute to the pathogenesis of inflammatory bowel disease. *Science*
1135 352: 1116–1120.

1136 63. Ramakrishna C, Kujawski M, Chu H, Li L, Mazmanian SK, Cantin EM. 2019.
1137 *Bacteroides fragilis* polysaccharide A induces IL-10 secreting B and T cells that
1138 prevent viral encephalitis. *Nature Communications* 10: 2153.

1139 64. Cameron EA, Kwiatkowski KJ, Lee B-H, Hamaker BR, Koropatkin NM, Martens
1140 EC. 2014. Multifunctional Nutrient-Binding Proteins Adapt Human Symbiotic
1141 Bacteria for Glycan Competition in the Gut by Separately Promoting Enhanced
1142 Sensing and Catalysis. *mBio* 5: e01441-14.

1143 65. Rogers TE, Pudlo NA, Koropatkin NM, Bell JS, Moya Balasch M, Jasker K,
1144 Martens EC. 2013. Dynamic responses of *Bacteroides thetaiotaomicron* during
1145 growth on glycan mixtures. *Molecular microbiology*, 2013/05/08 ed. 88: 876–90.

1146 66. Tartera C, Araujo R, Michel T, Jofre J. 1992. Culture and decontamination methods
1147 affecting enumeration of phages infecting *Bacteroides fragilis* in sewage. *Applied*
1148 *and environmental microbiology*, 1992/08/01 ed. 58: 2670–3.

1149 67. Hryckowian AJ, Merrill BD, Porter NT, Van Treuren W, Nelson EJ, Garlena RA,
1150 Russell DA, Martens EC, Sonnenburg JL. 2020. *Bacteroides thetaiotaomicron*-
1151 Infecting Bacteriophage Isolates Inform Sequence-Based Host Range Predictions.
1152 *Cell Host & Microbe* 28: 371–379.

1153 68. Koropatkin N, Martens EC, Gordon JI, Smith TJ. 2009. Structure of a SusD
1154 homologue, BT1043, involved in mucin O-glycan utilization in a prominent human
1155 gut symbiont. *Biochemistry*, 2009/02/05 ed. 48: 1532–42.

1156 69. Livak KJ, Schmittgen TD. 2001. Analysis of Relative Gene Expression Data Using
1157 Real-Time Quantitative PCR and the 2−ΔΔCT Method. *Methods* 25: 402–408.

1158 70. Ostrowski MP, La Rosa SL, Kunath BJ, Robertson A, Pereira G, Hagen LH,
1159 Varghese NJ, Qiu L, Yao T, Flint G, Li J, McDonald SP, Buttner D, Pudlo NA,
1160 Schnizlein MK, Young VB, Brumer H, Schmidt TM, Terrapon N, Lombard V,
1161 Henrissat B, Hamaker B, Eloe-Fadrosh EA, Tripathi A, Pope PB, Martens EC.
1162 2022. Mechanistic insights into consumption of the food additive xanthan gum by
1163 the human gut microbiota. *Nature Microbiology* 7: 556–569.

1164 71. Xu J. 2003. A Genomic View of the Human-*Bacteroides thetaiotaomicron*
1165 Symbiosis. *Science* 299: 2074–2076.

1166

Figure 1

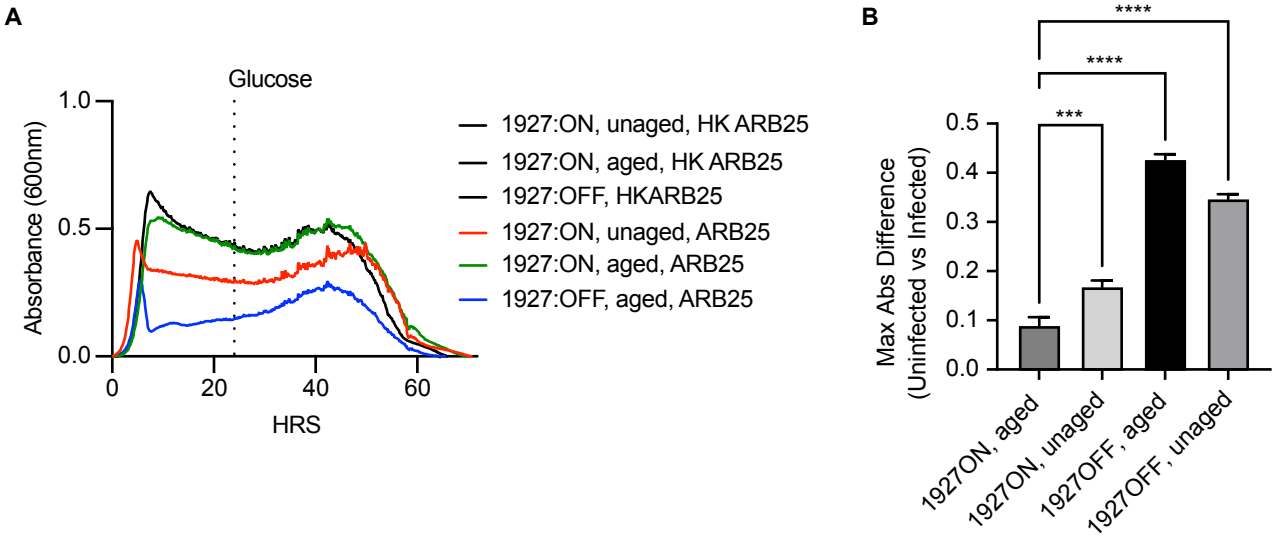
A
Glucose
1.0
0.5
0.0
Absorbance (600nm)
0
20
40
60
HRS
1927:ON, unaged, HK ARB25
1927:ON, aged, HK ARB25
1927:OFF, HKARB25
1927:ON, unaged, ARB25
1927:ON, aged, ARB25
1927:OFF, aged, ARB25
B
****
****
***
0.5
0.4
0.3
0.2
0.1
0.0
Max Abs Difference
(Uninfected vs Infected)
1927ON, aged
1927ON, unaged
1927OFF, aged
1927OFF, unaged

Figure 2

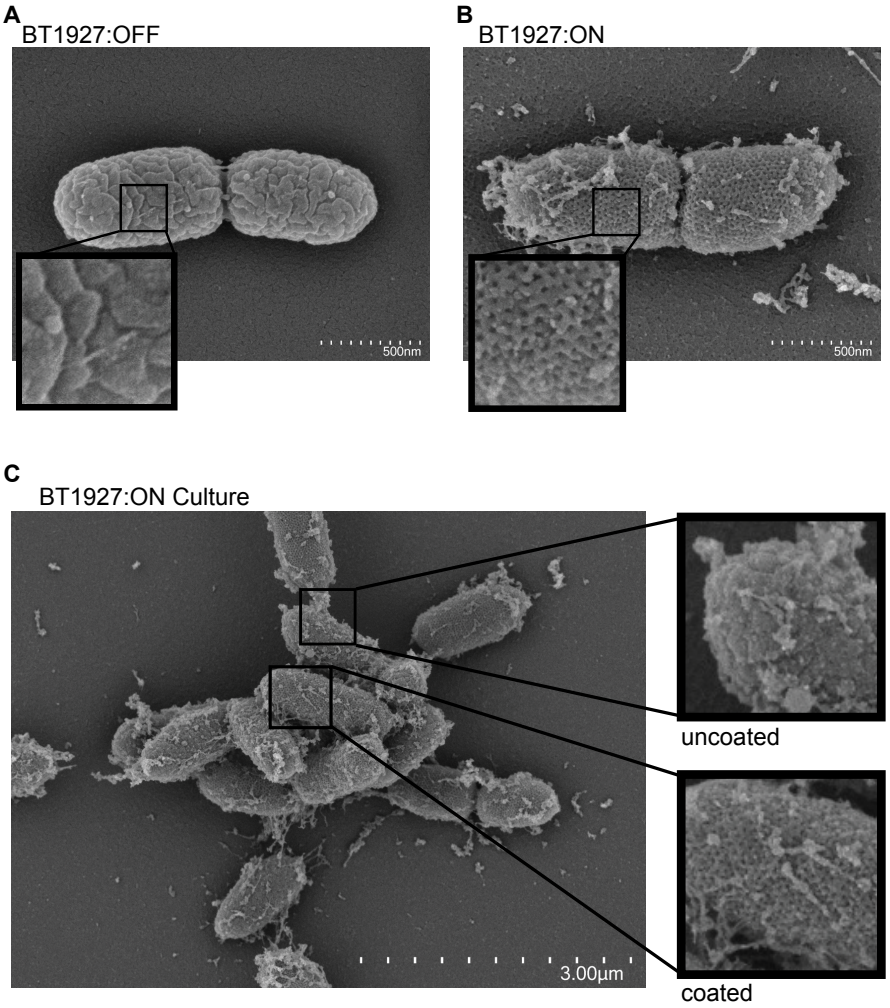
A
BT1927:OFF
500nm
B
BT1927:ON
500nm
C
BT1927:ON Culture
3.00µm
uncoated
coated

Figure 3

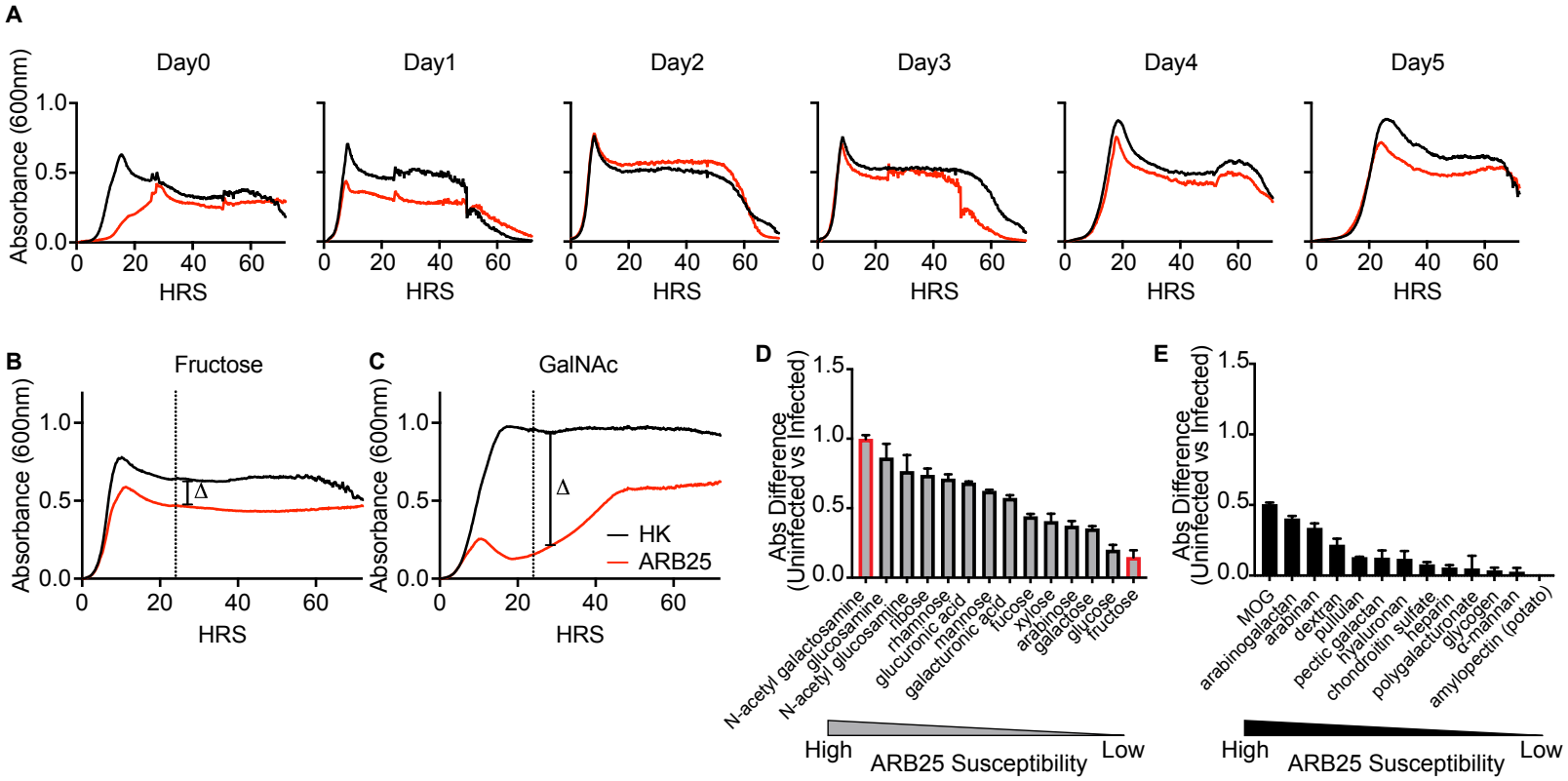
A
Day0
Day1
Day2
Day3
Day4
Day5
Absorbance (600nm)
HRS
B
Fructose
C
GalNAc
Δ
HK
ARB25
D
Abs Difference (Uninfected vs Infected)
N-acetyl galactosamine
glucosamine
N-acetyl glucosamine
ribose
rhamnose
glucuronic acid
mannose
galacturonic acid
fucose
xylose
arabinose
galactose
glucose
fructose
High
ARB25 Susceptibility
Low
E
MOG
arabinogalactan
arabinan
dextran
pullulan
pectic galactan
hyaluronan
chondroitin sulfate
heparin
polygalacturonate
glycogen
α-mannan
amylopectin (potato)

Figure 4

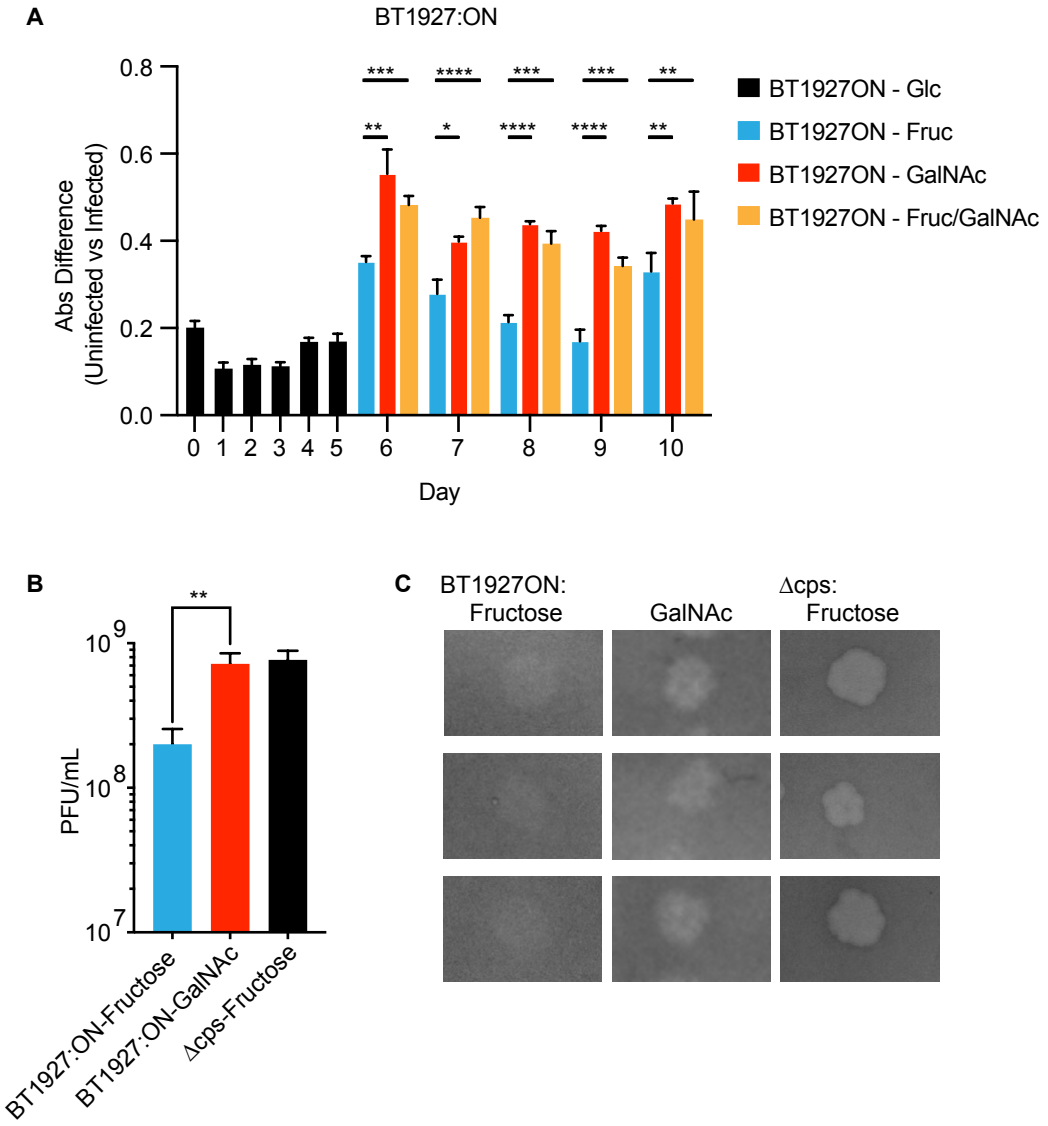
A
BT1927:ON
Abs Difference
(Uninfected vs Infected)
0.8
0.6
0.4
0.2
0.0
0 1 2 3 4 5 6 7 8 9 10
Day
***
****
***
***
**
**
*
****
****
**
BT1927ON - Glc
BT1927ON - Fruc
BT1927ON - GalNAc
BT1927ON - Fruc/GalNAc
B
**
PFU/mL
10^9
10^8
10^7
BT1927:ON-Fructose
BT1927:ON-GalNAc
Δcps-Fructose
C
BT1927ON:
Fructose
GalNAc
Δcps:
Fructose

Figure 5

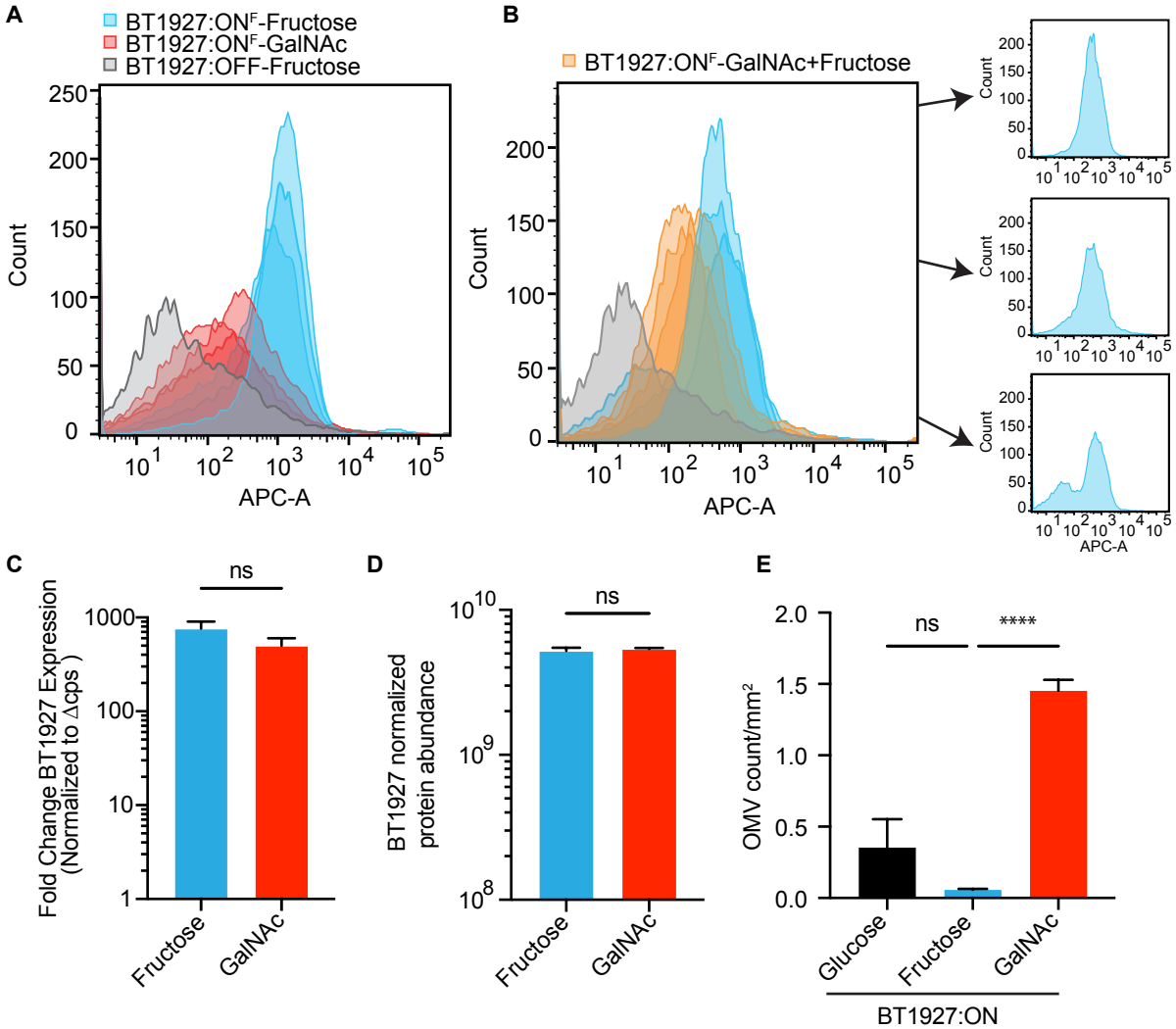
A
BT1927:ON^F-Fructose
BT1927:ON^F-GalNAc
BT1927:OFF-Fructose
Count
APC-A
B
BT1927:ON^F-GalNAc+Fructose
Count
APC-A
C
ns
Fold Change BT1927 Expression (Normalized to Δcps)
Fructose
GalNAc
D
ns
BT1927 normalized protein abundance
Fructose
GalNAc
E
ns
****
OMV count/mm²
Glucose
Fructose
GalNAc
BT1927:ON

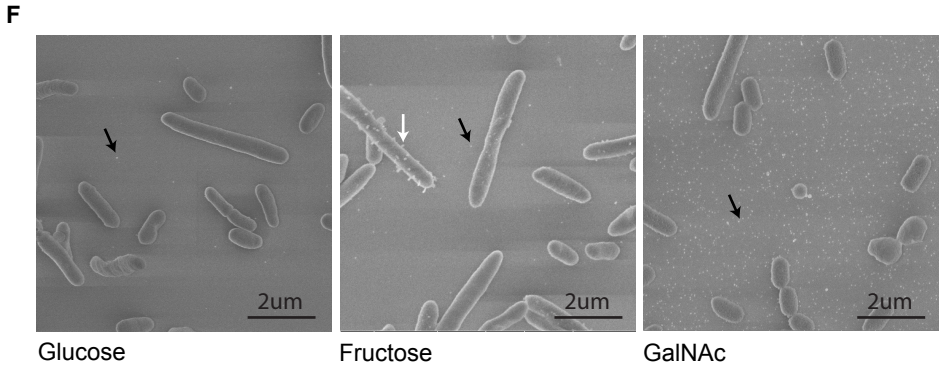
F
2um
2um
2um
Glucose
Fructose
GalNAc

Figure 6

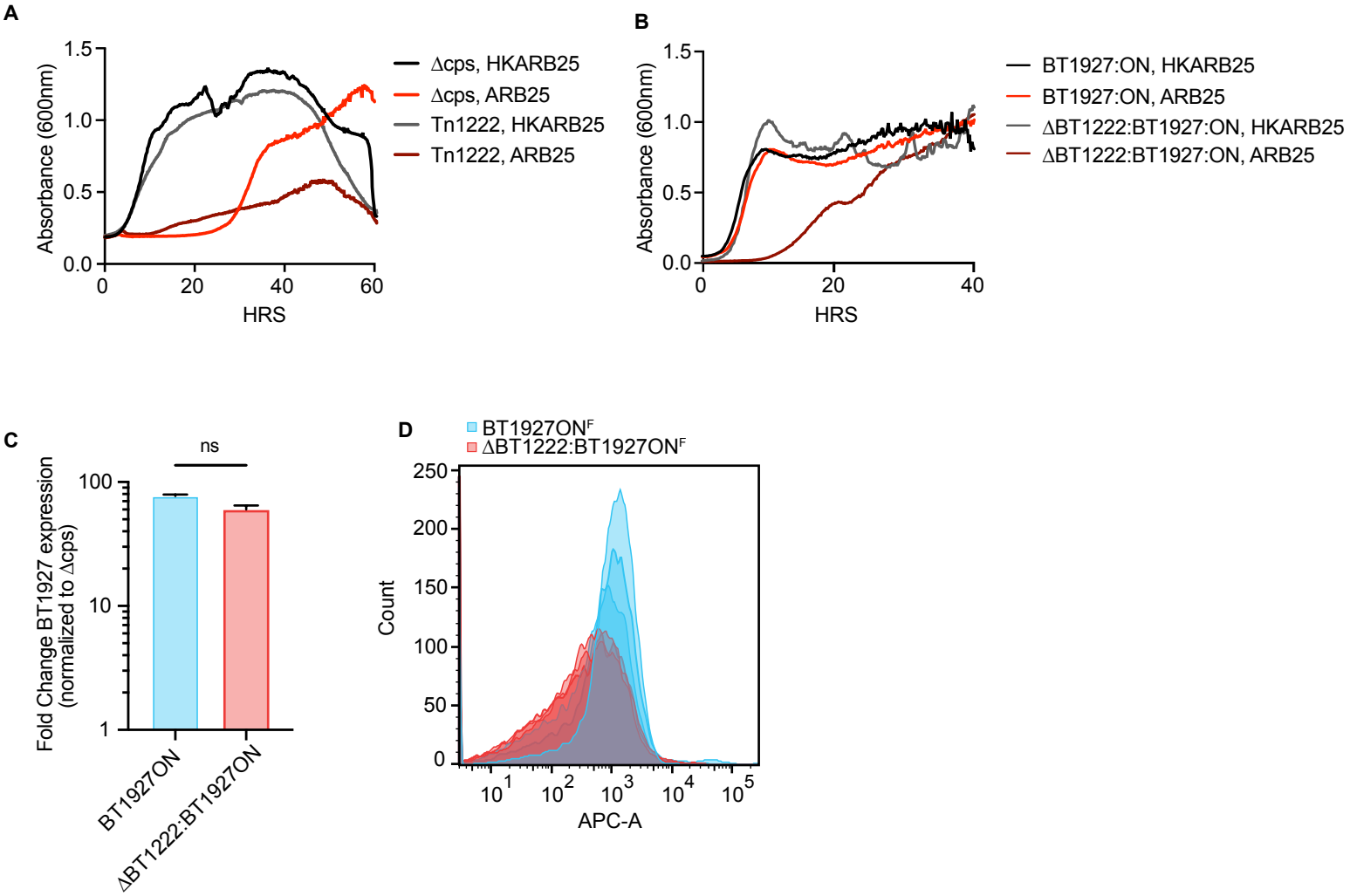
A
Absorbance (600nm)
HRS
Δcps, HKARB25
Δcps, ARB25
Tn1222, HKARB25
Tn1222, ARB25
B
Absorbance (600nm)
HRS
BT1927:ON, HKARB25
BT1927:ON, ARB25
ΔBT1222:BT1927:ON, HKARB25
ΔBT1222:BT1927:ON, ARB25
C
ns
Fold Change BT1927 expression (normalized to Δcps)
BT1927ON
ΔBT1222:BT1927ON
D
BT1927ON^F
ΔBT1222:BT1927ON^F
Count
APC-A

Figure S1

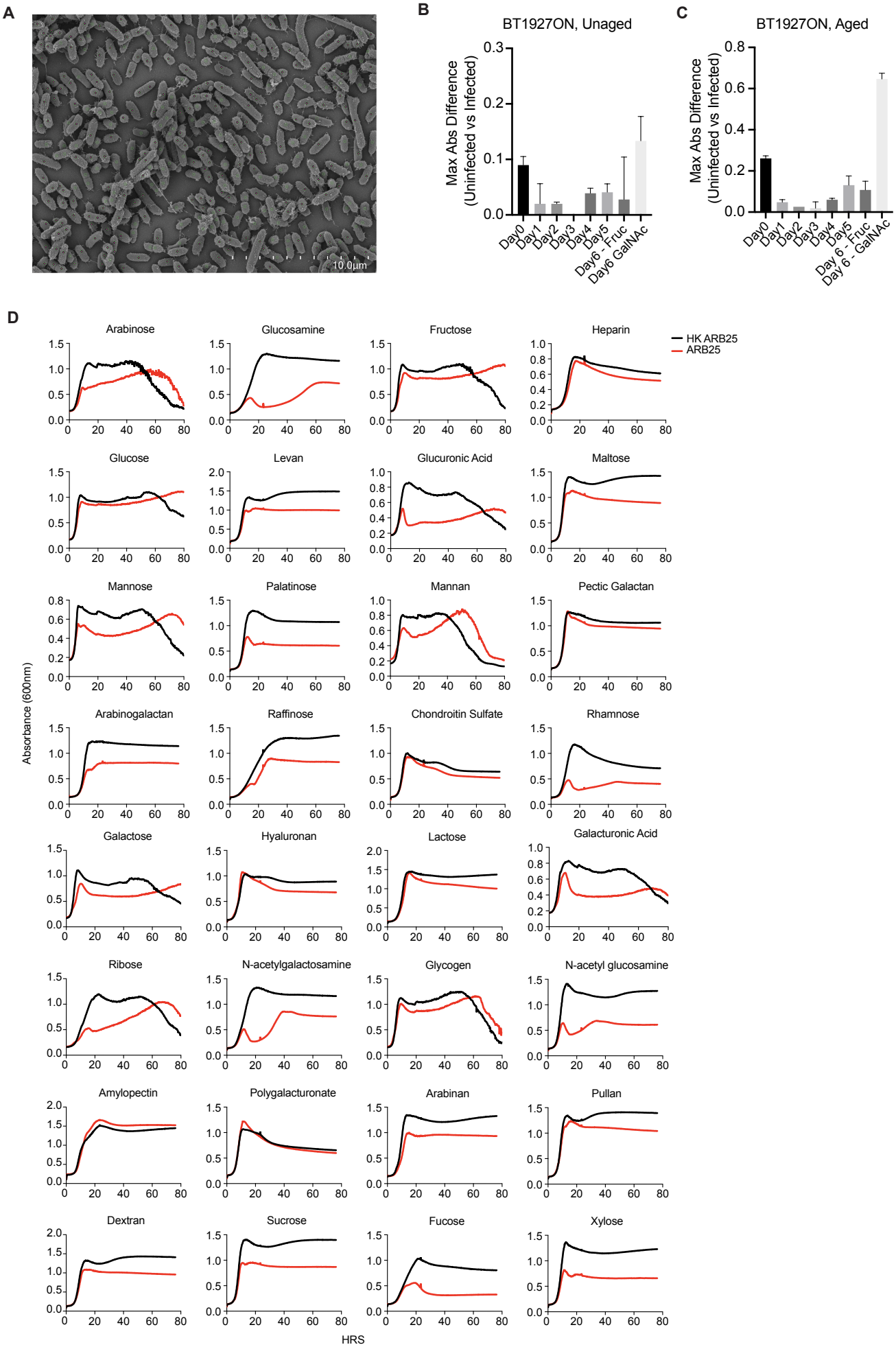
A
10.0µm
B
BT1927ON, Unaged
Max Abs Difference (Uninfected vs Infected)
Day0
Day1
Day2
Day3
Day4
Day5
Day6 - Fruc
Day6 GalNAc
C
BT1927ON, Aged
Max Abs Difference (Uninfected vs Infected)
Day0
Day1
Day2
Day3
Day4
Day5
Day 6 - Fruc
Day 6 - GalNAc
D
HK ARB25
ARB25
Absorbance (600nm)
HRS
Arabinose
Glucosamine
Fructose
Heparin
Glucose
Levan
Glucuronic Acid
Maltose
Mannose
Palatinose
Mannan
Pectic Galactan
Arabinogalactan
Raffinose
Chondroitin Sulfate
Rhamnose
Galactose
Hyaluronan
Lactose
Galacturonic Acid
Ribose
N-acetylgalactosamine
Glycogen
N-acetyl glucosamine
Amylopectin
Polygalacturonate
Arabinan
Pullan
Dextran
Sucrose
Fucose
Xylose

Figure S2

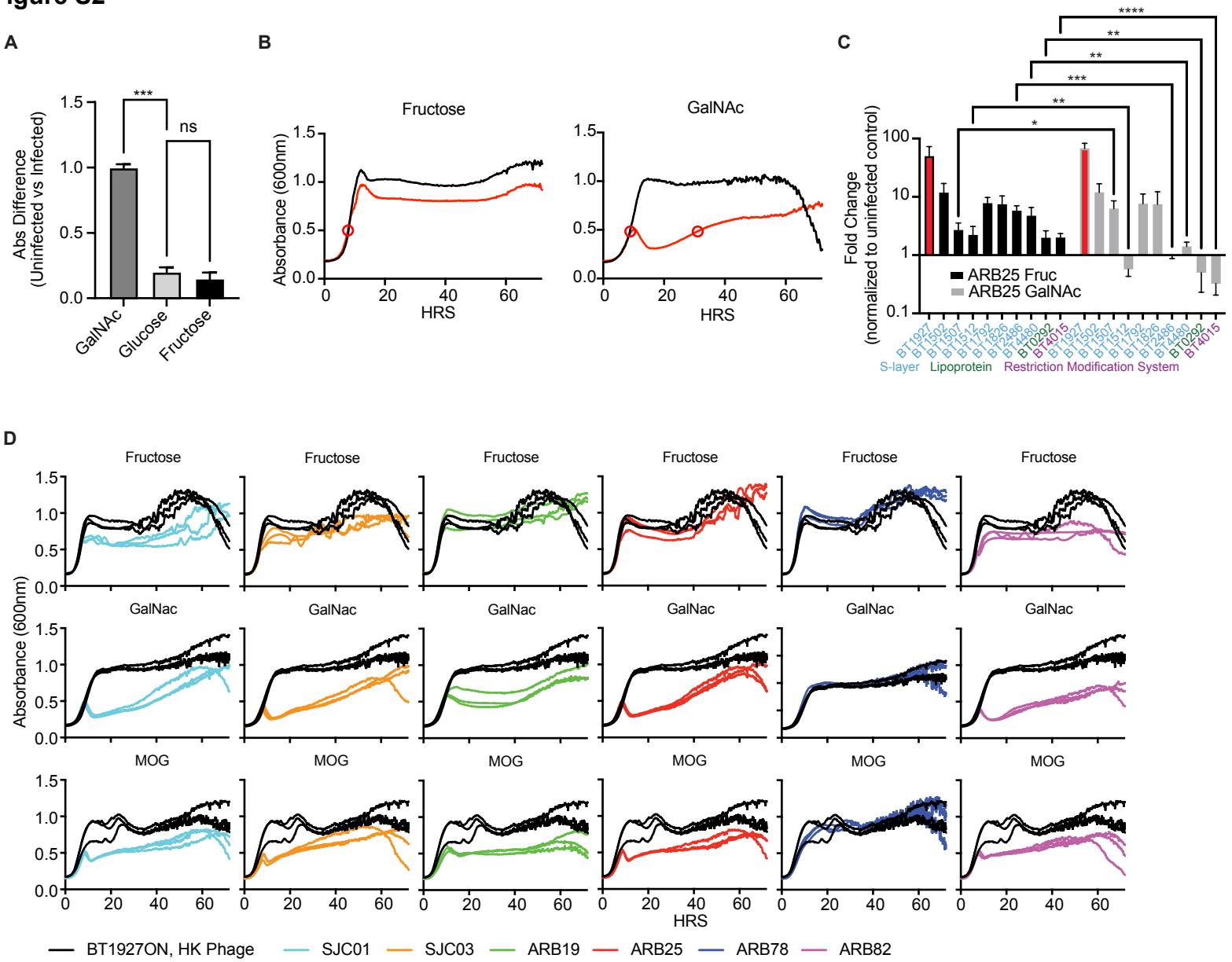
A
Abs Difference (Uninfected vs Infected)
***
ns
GalNAc
Glucose
Fructose
B
Fructose
GalNAc
Absorbance (600nm)
HRS
C
Fold Change (normalized to uninfected control)
ARB25 Fruc
ARB25 GalNAc
S-layer
Lipoprotein
Restriction Modification System
D
Fructose
GalNac
MOG
Absorbance (600nm)
HRS
BT1927ON, HK Phage
SJC01
SJC03
ARB19
ARB25
ARB78
ARB82

Figure S3

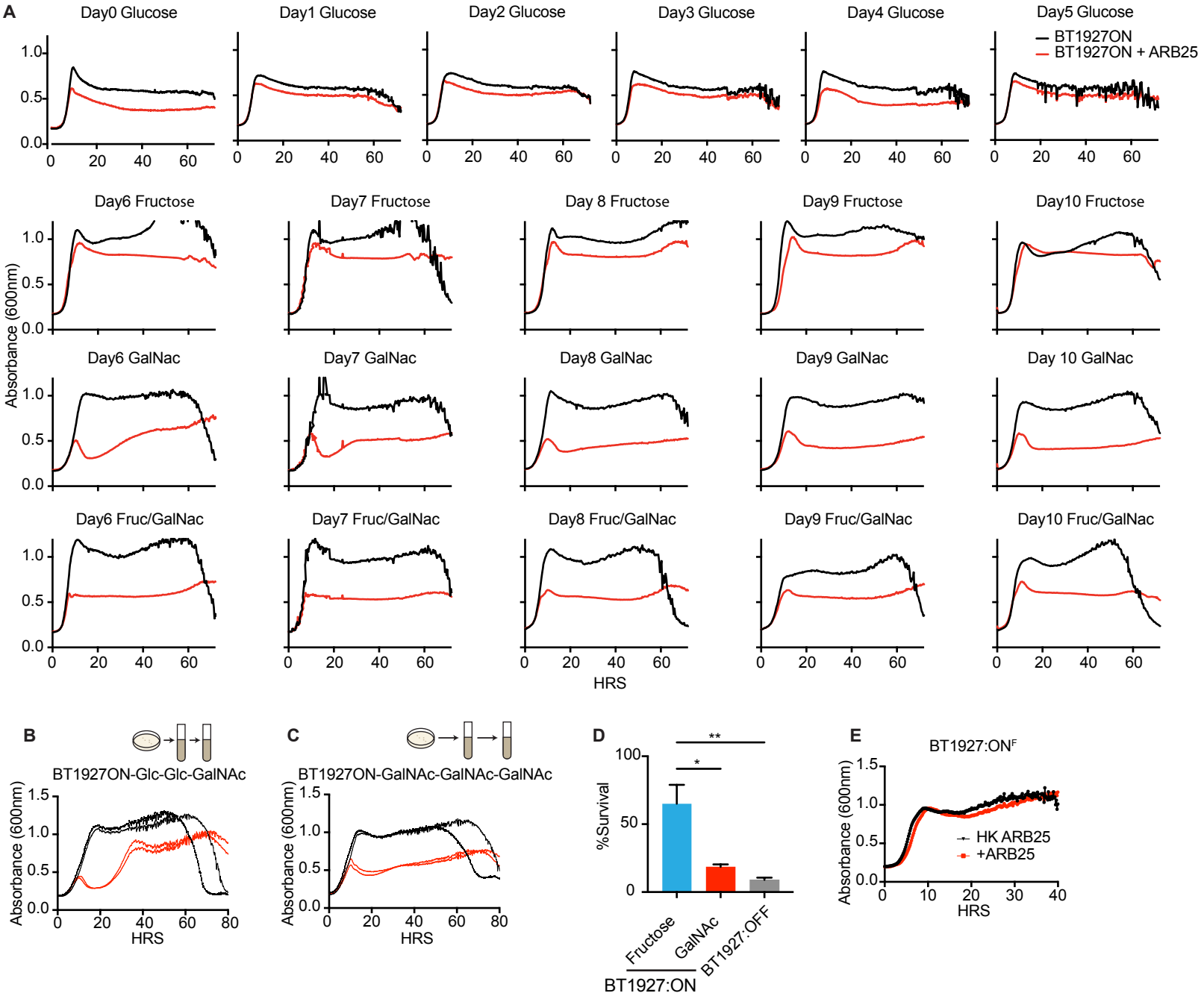
A
Day0 Glucose
Day1 Glucose
Day2 Glucose
Day3 Glucose
Day4 Glucose
Day5 Glucose
BT1927ON
BT1927ON + ARB25
Day6 Fructose
Day7 Fructose
Day 8 Fructose
Day9 Fructose
Day10 Fructose
Day6 GalNac
Day7 GalNac
Day8 GalNac
Day9 GalNac
Day 10 GalNac
Day6 Fruc/GalNac
Day7 Fruc/GalNac
Day8 Fruc/GalNac
Day9 Fruc/GalNac
Day10 Fruc/GalNac
Absorbance (600nm)
HRS
B
BT1927ON-Glc-Glc-GalNAc
Absorbance (600nm)
HRS
C
BT1927ON-GalNAc-GalNAc-GalNAc
Absorbance (600nm)
HRS
D
%Survival
Fructose
GalNAc
BT1927:OFF
BT1927:ON
E
BT1927:ON^F
Absorbance (600nm)
HK ARB25
+ARB25
HRS

Figure S4

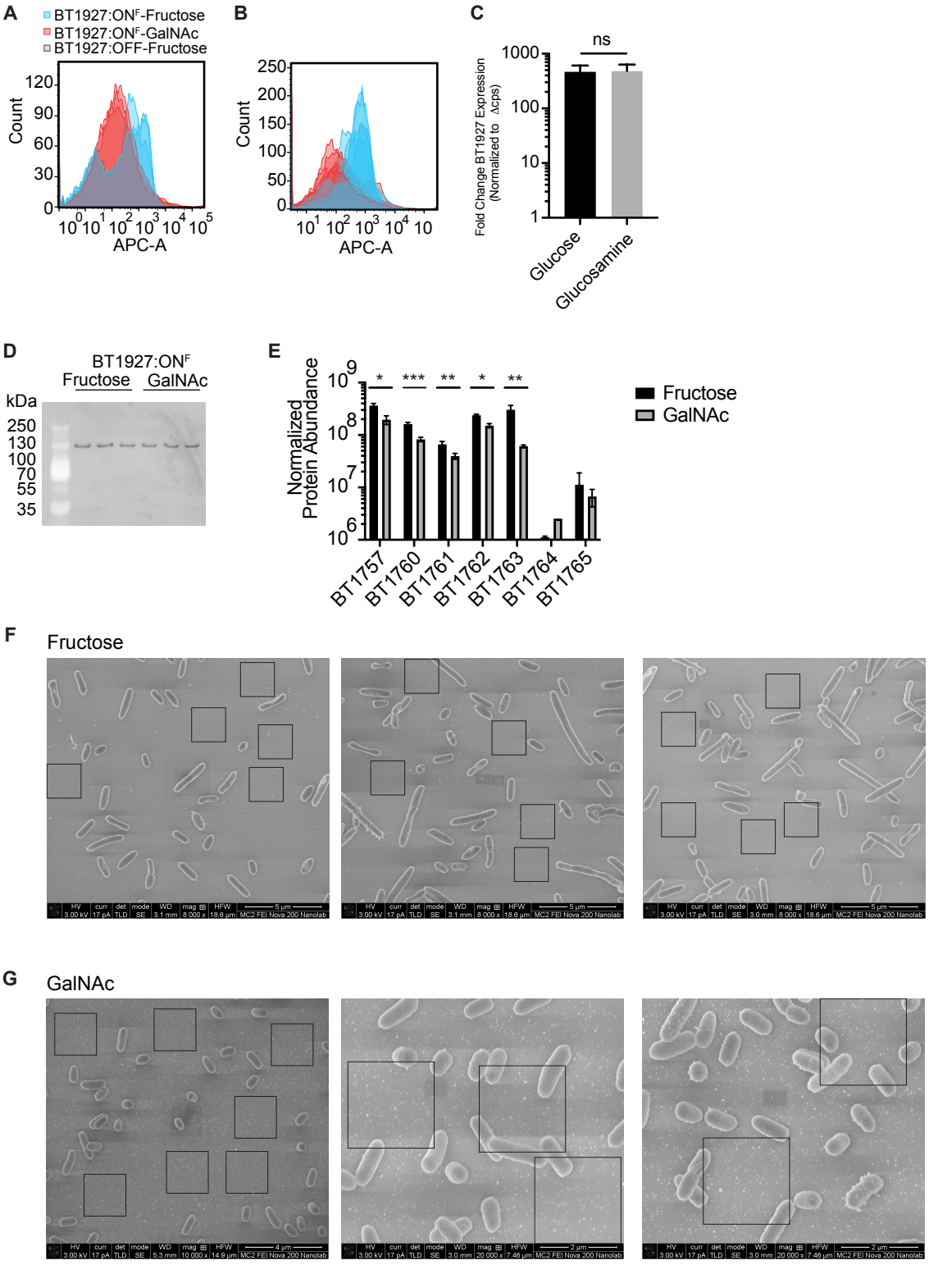
A
BT1927:ON^F-Fructose
BT1927:ON^F-GalNAc
BT1927:OFF-Fructose
Count
APC-A
B
Count
APC-A
C
ns
Fold Change BT1927 Expression (Normalized to Δcps)
Glucose
Glucosamine
D
BT1927:ON^F
Fructose
GalNAc
kDa
250
130
100
70
55
35
E
Normalized Protein Abundance
Fructose
GalNAc
BT1757
BT1760
BT1761
BT1762
BT1763
BT1764
BT1765
F
Fructose
G
GalNAc

Figure S5

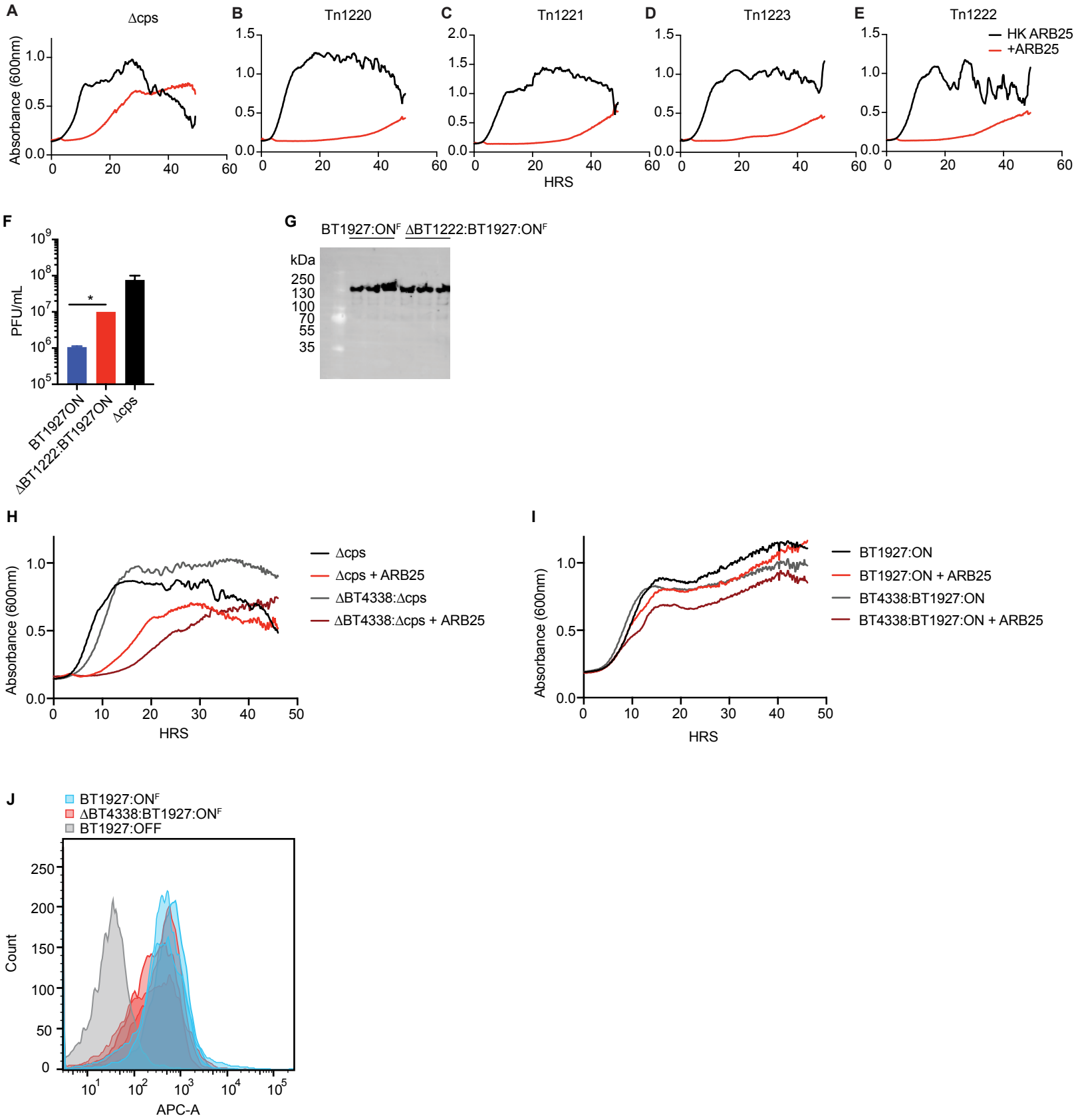
A
Δcps
B
Tn1220
C
Tn1221
D
Tn1223
E
Tn1222
HK ARB25
+ARB25
Absorbance (600nm)
HRS
F
PFU/mL
BT1927ON
ΔBT1222:BT1927ON
Δcps
G
BT1927:ON^F
ΔBT1222:BT1927:ON^F
kDa
250
130
100
70
55
35
H
Δcps
Δcps + ARB25
ΔBT4338:Δcps
ΔBT4338:Δcps + ARB25
Absorbance (600nm)
HRS
I
BT1927:ON
BT1927:ON + ARB25
BT4338:BT1927:ON
BT4338:BT1927:ON + ARB25
Absorbance (600nm)
HRS
J
BT1927:ON^F
ΔBT4338:BT1927:ON^F
BT1927:OFF
Count
APC-A